A generalization of the achievable rate of a MISO system using Bode-Fano wideband matching theory

Nitish Deshpande, *Student Member, IEEE,* Miguel R. Castellanos, *Member, IEEE,* Saeed R. Khosravirad, *Senior Member, IEEE,* Jinfeng Du, *Senior Member, IEEE,* Harish Viswanathan, *Fellow, IEEE,* and Robert W. Heath Jr., *Fellow, IEEE*

***Abstract*—Impedance-matching networks affect power transfer from the radio frequency (RF) chains to the antennas. Their design impacts the signal to noise ratio (SNR) and the achievable rate. In this paper, we maximize the information-theoretic achievable rate of a multiple-input-single-output (MISO) system with wideband matching constraints. Using a multiport circuit theory approach with frequency-selective scattering parameters, we propose a general framework for optimizing the MISO achievable rate that incorporates Bode-Fano wideband matching theory. We express the solution to the achievable rate optimization problem in terms of the optimized transmission coefficient and the Lagrangian parameters corresponding to the Bode-Fano inequality constraints. We apply this framework to a single electric Chu's antenna and an array of dipole antennas. We compare the optimized achievable rate obtained numerically with other benchmarks like the ideal achievable rate computed by disregarding matching constraints and the achievable rate obtained by using sub-optimal matching strategies like conjugate matching and frequency-flat transmission. We also propose a practical methodology to approximate the achievable rate bound by using the optimal transmission coefficient to derive a physically realizable matching network through the ADS software.**

***Index Terms*—Bode-Fano matching theory, achievable rate maximization, scattering parameters, matching network design**

I. Introduction

As wireless systems exploit higher bandwidths, it is crucial to design matching networks that support the desired power transfer in the band of interest to achieve the target data rate [1]–[4]. For narrowband systems, matching networks are optimized for power transfer between source and load at a single frequency. For wideband arrays, it is challenging to design matching networks because the load depends on the frequency-selectivity of the array including mutual coupling between antennas [4]. The Bode-Fano theory captures these practical matching constraints with a frequency-selective circuit theory approach based on scattering parameters [2], [5]. In this paper, we incorporate these constraints in achievable rate analysis unlike conventional wideband MIMO literature which does not treat matching networks as a part of the analysis [6], [7].

The problem of matching a source impedance to a load impedance in conventional RF literature is mostly based on power transfer based metrics [5], [8]–[11]. In general, the transmit matching network is designed to maximize power transfer efficiency while the receive matching network to minimize the noise figure. For a narrowband system, the conjugate matching network is designed such that the effective load impedance equals complex conjugate of the source impedance. For broadband matching, the constant quality factor circle technique can be used [5]. Designing matching networks for systems operating at higher fractional bandwidths is challenging because of the frequency-selectivity of the load. Recently, a globally optimal approach to designing wideband matching networks defined a unique trajectory connecting source and load on Smith chart using the power transfer efficiency metric [10]. Although power transfer efficiency is important, it only quantifies the power transfer from the RF chain to the antennas within a transmitter. From a communication theoretic perspective, the most relevant metric is the end-to-end achievable data rate. The communication rate depends on factors like the bandwidth, wireless propagation channel, beamforming response at both receiver and transmitter, mutual coupling between antenna elements, and their radiation patterns. The achievable rate metric captures all factors. Hence, wireless devices should optimize the matching network to maximize the rate rather than the power transfer efficiency.

For analysis of wideband systems, it is essential to understand the fundamental design tradeoffs between gain and bandwidth [12]. In large phased-arrays operating at higher fractional bandwidths, there is a phase mismatch between the frequency-flat phase-shifter and frequency-selective array response [13]. The frequency-selectivity of antennas and matching networks was considered for analysis of dense array wideband massive MIMO [14]. The results in [14], [15] showed that for systems which use matching networks based on the conjugate matching strategy, the SNR drops drastically for frequencies away from the center frequency. A matching network based on a narrowband assumption is sub-optimal in a wideband setting. Hence, it is necessary to optimize physically realizable matching networks over the bandwidth of interest. These examples show that the shift from frequency-flat to frequency-selective models is necessary as wireless systems transition from narrowband to wideband operation [12]–[16].

The circuit theory approach to modeling wireless commu-

Nitish Deshpande and Robert W. Heath Jr. are with the Department of Electrical and Computer Engineering, University of California San Diego, La Jolla, CA 92093 (email: {nideshpande, rwheathjr}@ucsd.edu). Miguel R. Castellanos is with North Carolina State University, Raleigh, NC 27606 USA (email: mrcastel@ncsu.edu). Saeed R. Khosravirad, Jinfeng Du, and Harish Viswanathan are with Nokia Bell Laboratories, Murray Hill, NJ 07974, USA (email: {saeed.khosravirad, jinfeng.du, harish.viswanathan}@nokia-bell-labs.com). This project is funded in part by Nokia Bell Laboratories, Murray Hill, NJ 07974, USA. This material is also based upon work supported in part by the National Science Foundation under Grant No. NSF-CNS-2147955 and NSF-ECCS-2153698 and by funds from federal agencies and industry partners from the Resilient & Intelligent NextG Systems program.

nication systems enables incorporating physically consistent frequency-selective models for the antennas, arrays, wireless channel, and the RF chain components in the analysis [17]. This approach captures effects like mutual coupling in the form of impedance or scattering matrices thus making the system analysis more realistic and tractable [4], [15], [17]–[24]. Although circuit theoretic abstractions have been used for decades for the design of individual RF components like antennas [25], [26], matching networks [5], and amplifiers [27], the application of circuit models for MIMO communication systems is more recent. Phenomena like super-directivity [19] and super-bandwidth [23] that occur in tightly coupled arrays can be explained with the circuit theory approach. Hardware effects like amplifier current constraints [14] and matching network limitations [15] can also be incorporated through circuit models. Hence, the circuit theory approach to communication is useful to design matching networks for optimizing achievable rate.

Prior work has studied achievable rate maximization through impedance-matching only for specific matching network topologies [4], [21], [22], [28], [29]. In [21], an upper bound on the MIMO-OFDM capacity was proposed by optimizing the receiver matching network parameters based on a T-network topology. In [4], the achievable rate of a MISO and SIMO system was optimized in terms of the inductances and transformer turns ratio of a single port matching network. Although [4] and [21] used a communication theoretic objective, the methods used for optimizing the matching network parameters are specific to a given topology and do not guarantee optimality over a general family of passive and linear matching networks.

From a circuit theory perspective, there exists a fundamental limit on the wideband performance of a passive matching network, popularly known as the Bode-Fano limits [5], [8], [9]. Recent work derived an upper bound on the single-input-single-output (SISO) achievable rate by applying the Bode-Fano wideband matching constraints at the receiver [22] and transmitter [30]. The main challenge for extending the achievable rate analysis in [22] and [30] to a MISO system includes incorporating the mutual coupling and analog beamforming network to derive the Bode-Fano upper bound required for optimizing the achievable rate. The optimization framework for a SISO system was limited to a fixed number of constraints. In MISO system, the number of constraints are dependent on the analog beamforming too which necessitates the generalization of the optimization framework to an arbitrary number of Bode-Fano constraints. Recently, a multiport extension of the Bode-Fano matching theory proposed new bounds applicable to a system with multiple transmit antennas driven by multiple sources [2], [31]. The application of the improved Bode-Fano matching limits to a MIMO system from an achievable rate perspective is not investigated in prior work. For the SISO case, the bounds in [22] and [30] were based on closed-form models for the Chu's antenna. In the present work, we extend such analysis to a generalized MISO system by leveraging advanced numerical tools such as MATLAB Antenna Toolbox, MATLAB RF Toolbox, and Keysight ADS.

In this paper, we analyze a MISO system from a joint circuit and communication theoretic perspective. We answer two fundamental questions. The first question is "What is the upper bound on the achievable rate of a MISO system over all physically realizable linear and passive matching networks that satisfy the Bode-Fano wideband matching constraints?" We demonstrate how ignoring the Bode-Fano constraints leads to an over-estimation of the rate for wideband systems. The second question is "How to design impedance-matching networks that achieve rate close to the proposed upper bound?" In contrast to prior work, we design realizable matching networks that maximize achievable rate. The main contributions of this paper are as follows.

- We derive a frequency-selective circuit theoretic model of a MISO system with a single RF chain at the transmitter that supplies power to the antenna array through an impedance-matching network and an analog beamforming network. This model is used in our proposed general framework for optimizing the achievable rate of wideband MISO systems. For deriving the constraints, we use a rational and passive approximation of the equivalent load comprising of the analog beamforming network and the transmit antennas. The maximum achievable rate is expressed in terms of the optimized transmission coefficient and Lagrangian parameters associated with the Bode-Fano inequalities.
- We propose a three step procedure to design circuits that approximate the desired optimal response obtained through the achievable rate optimization solution. Our simulation results show that the matching network designed using this procedure achieves rates close to the maximum achievable rate bound. We demonstrate this three step procedure for two specific models: a single Chu's electric antenna and an array of dipole antennas. We use a practical LC ladder matching network topology whose components are numerically optimized in ADS to fit the corresponding optimal transmission coefficient.
- We compare our proposed bound and the performance of the designed matching network with the ideal Shannon's bound, frequency-flat transmission, conjugate matching at center frequency, and the no matching case. We also analyze the achievable rate trend with bandwidth. We show the existence of an optimal bandwidth for the achievable rate bound obtained with Bode-Fano constraints and the corresponding circuit simulations.
- We show that the achievable rate performance can be further improved for higher bandwidths by optimally designing the transmit power spectral density using a water-filling approach instead of equal power allocation for all frequencies. Through simulations, we show that the insights and bandwidth trends are also generalizable to the case where impact of receiver matching network and intrinsic noise is included in the receiver model.

This paper is organized as follows: In Section II, we discuss the choice of the modeling framework in comparison with other frameworks used in literature. Choosing a circuit theoretic modeling methodology, we formulate a frequency-selective model for a MISO system where the linear network

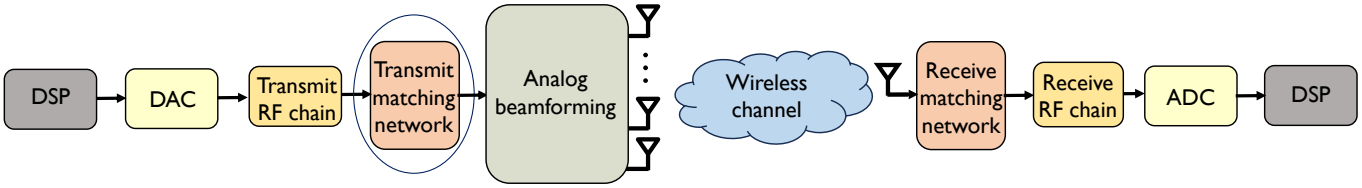

Fig. 1: A diagram of the considered multi-antenna transmitter and single-antenna receiver. In this paper, the focus is on designing the transmit matching network to maximize achievable rate.

parameters are described using the scattering parameter notation. In Section III, we discuss the general form of the Bode-Fano matching constraints followed by the achievable rate optimization problem formulation and derivation of the optimal transmission coefficient. In Section IV, we propose a methodology to design matching networks based on the derived transmission coefficient supported by circuit illustrations using ADS software. In Section V, we present numerical results for SNR and achievable rate using the derived theoretical bounds, circuit simulations, and comparison with conventional matching benchmarks. In Section VI, we summarize the key takeaways and discuss future research directions. The simulation code for generating achievable rate optimization results and the corresponding circuit ADS files are made publicly available to facilitate reproducibility[1].

Notation: A bold lowercase letter $\mathbf{a}$ denotes a column vector, a bold uppercase letter $\mathbf{A}$ denotes a matrix, $(\cdot)^*$ denotes conjugate, $(\cdot)^T$ denotes transpose, $|\cdot|$ indicates absolute value, $\mathbf{I}_N$ represents the identity matrix of size N, $\mathbf{0}_N$ represents an all zero matrix of size N, $\mathcal{R}(z)$ denotes the real part of a complex number z, $\{i\}_1^N$ is shorthand for $i = \{1, 2, \ldots, N\}$, $[z]^+ = \max(0, z)$.

II. System model

A. Modeling frameworks for wireless communication system

With every wireless generation, there has been evolution in the communication system modeling approach. The analysis of a wireless system is impacted by the choice of model. It is important to choose a model that encompasses the proper assumptions and ensures the validity and applicability of the insights to the target wireless application.

We overview different frameworks that are used for modeling physical layer wireless communication. In terms of frequency dependence, the system model is classified as frequency-flat or frequency-selective. For frequency-flat models, the network parameters are evaluated at a specific center frequency and assumed to be fixed over the narrow bandwidth of interest. For narrowband wireless applications like sensor networks, RFID [32], and narrowband Internet of Things [33], it suffices to use a frequency-flat modeling framework. For wideband wireless applications like satellite communication, Wi-Fi, and cellular [34], frequency-selective models are required to guarantee that the analytical or numerical results from the model are useful for the desired frequency range.

In terms of the modeling methodology, the models can be classified as dimensionless (non-circuit theoretic models) and physically consistent (circuit theoretic models). Non-circuit theoretic models have been useful for analyzing achievable rate, interference analysis, power allocation [7], and beamforming optimization. However, the definition of power with these models is based on a single complex dimensionless variable. The power definition using circuit models is based on a pair of variables like the current and voltage or incident and reflected root power waves [17], [5]. For problems like impedance-matching network design which relate to power flow [4], or analysis of new array architectures like dynamic metasurface antennas [35], it is essential to use a circuit model to capture the relevant hardware and electromagnetic effects like mutual coupling [20] and polarization [36].

The circuit theoretic MIMO models can be further classified based on impedance/admittance versus scattering parameters. Although impedance and scattering parameters can be converted to each other through algebraic transformations, the scattering parameters are more applicable because they can be easily measured for any general load and directly relate to the flow of power [5]. Scattering parameters are widely recognized in the RF community for design of individual RF components like antennas [26], matching networks [5], and amplifiers [27]. The use of scattering parameters for the analysis of wireless communication systems allows us to leverage several results on matching network analysis developed in the microwave and antenna community [2], [31]. It also makes our work generalizable to any practical RF system. As we target the achievable rate analysis and matching network design problem for wideband systems, we use the circuit theoretic frequency-selective model with scattering parameters.

B. A two-port linear network model of communication system

In Fig. 1, we present the MISO communication system model. The conventional MISO communication system representation includes DSP, DAC, transmit RF chain, analog beamforming, and multiple antennas at the transmitter whereas the receiver includes receive RF chain, ADC, and DSP. Besides these typical components, we include the transmit and receive matching network in this representation. The focus of this paper is on transmit matching network which is an important component in a communication link. In Fig. 2(a), we provide an abstraction of the communication system with a single source and single load using a two-port network model [22]. On the transmitter side, the source generates the transmit signal obtained from the output of the transmit RF chain, i.e., the signal obtained after up-conversion and amplification. This signal is input to a cascade of linear networks effectively

[1]https://github.com/nvdeshpa/AchievableRateWidebandMatching

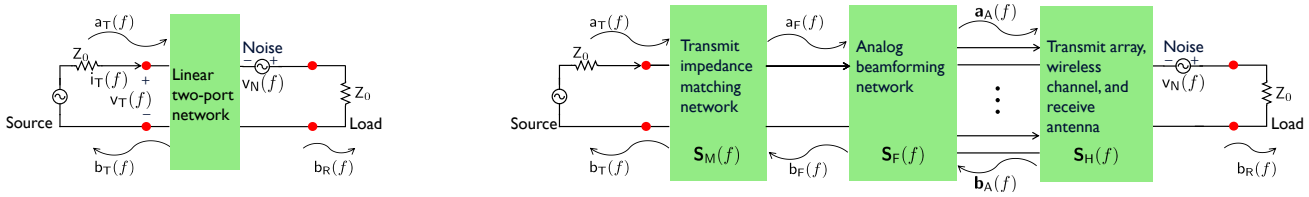

Fig. 2: In (a), a communication system with one RF chain at both receiver and transmitter is modeled as a two-port network. In (b), the two-port network model is specified for a MISO system with one transmit RF chain connected to N antennas through impedance-matching network and analog beamforming network.

modeled as a linear two-port network. The two-port network is used to model several linear blocks of a communication system like the impedance-matching network, analog beamforming network, transmit antenna array network, wireless propagation channel, and receive antenna as shown in Fig. 2(b) and described in Section II-C. We model the noise contribution from background radiation at the receive antenna by a voltage source at the output of the linear two-port network [17]. The receiver RF chain is modeled as a load. For simplifying the analysis in Section III, we do not model the low noise amplifier (LNA), receive matching network, and intrinsic noise source. In Section V-D, we investigate the impact of LNA and intrinsic noise sources through simulations and show that the insights from Section III are also valid for a practical receiver model.

We use a frequency domain representation for describing the signal flow through the two-port network. The subscript "T" indicates transmitted signal while subscript "R" indicates received signal. Let the voltage of the real-valued passband transmit signal in time domain at the input of the two-port network be $v_{\mathsf{T}}(t)$. Let the current entering the two-port network be $i_{\mathsf{T}}(t)$. We assume that the stochastic signals $v_{\mathsf{T}}(t)$ and $i_{\mathsf{T}}(t)$ are Gaussian wide-sense stationary random processes so that these signals are completely described by their mean and second-order moments [37]. As these signals do not have finite energy, a windowed Fourier transform with interval T_0 is used for defining the spectrum [38]. For frequency domain representation, we use frequency f in Hertz. Let the frequency domain voltage and current be defined as

$$\mathsf{v}_{\mathsf{T}}(f) = \int_{-\frac{T_0}{2}}^{\frac{T_0}{2}} v_{\mathsf{T}}(t) e^{-\mathrm{j}2\pi f t} \mathrm{d}t \left[\frac{\mathrm{V}}{\mathrm{Hz}}\right], \tag{1a}$$

$$\mathsf{i}_{\mathsf{T}}(f) = \int_{-\frac{T_0}{2}}^{\frac{T_0}{2}} i_{\mathsf{T}}(t) e^{-\mathrm{j}2\pi f t} \mathrm{d}t \left[\frac{\mathrm{A}}{\mathrm{Hz}}\right]. \tag{1b}$$

The main purpose of using the frequency domain representation is to simplify the analysis.

For further simplification, we use a root power wave representation of the signals which directly relates to the flow of power [5]. The root power waves at different ports are related by the scattering parameters, which can be easily measured compared to impedance or admittance parameters. The root power wave is a stochastic process which can be expressed as a linear combination of the current and voltage stochastic processes. In terms of the voltage and current, assuming characteristic impedance of the transmit circuit as Z_0, the root power wave incident on the two-port network is defined as [5, Eq 2.118]

$$\mathsf{a}_{\mathsf{T}}(f) = \frac{\mathsf{v}_{\mathsf{T}}(f) + \mathsf{Z}_0 \mathsf{i}_{\mathsf{T}}(f)}{2\sqrt{\mathcal{R}\{\mathsf{Z}_0\}}} \left[\frac{\sqrt{\mathrm{W}}}{\mathrm{Hz}}\right]. \tag{2}$$

The root power wave reflected back from the two-port network on the transmit side is defined as [5, Eq 2.118]

$$\mathsf{b}_{\mathsf{T}}(f) = \frac{\mathsf{v}_{\mathsf{T}}(f) - \mathsf{Z}_0^* \mathsf{i}_{\mathsf{T}}(f)}{2\sqrt{\mathcal{R}\{\mathsf{Z}_0\}}} \left[\frac{\sqrt{\mathrm{W}}}{\mathrm{Hz}}\right]. \tag{3}$$

The power spectral density of the power incident (or available) on the transmitter side of the two-port network is [5], [22]

$$P_{\mathsf{T}}(f) = \lim_{T_0 \to \infty} \frac{1}{T_0} \mathbb{E}[|\mathsf{a}_{\mathsf{T}}(f)|^2] \left[\frac{\mathrm{W}}{\mathrm{Hz}}\right]. \tag{4}$$

Although currents and voltage signals can be used for formulating the communication system model, the root power wave notation is a good mathematical tool for simplifying the impedance-matching problem in terms of metrics like power loss ratio and transmission coefficient [39].

On the receiver side, we assume an ideal load termination Z_0 to avoid reflected root power wave from the load and simplify the analysis. This load termination requires the use of a receive matching network that transfers all incident power to the receive RF chain. The modeling of a practical receive matching network was done in [22] while we focus only on the practical transmit matching network analysis and design. The root power wave at the output of the linear two-port network represents the received signal component $\mathsf{b}_{\mathsf{RS}}(f)$. The voltage source at the receiver port models the noise from background radiation. The noise voltage source is denoted as $\mathsf{v}_{\mathsf{N}}(f)$. The resulting root power wave is [20]

$$\mathsf{b}_{\mathsf{RN}}(f) = \frac{\mathsf{v}_{\mathsf{N}}(f)}{\sqrt{\mathcal{R}\{\mathsf{Z}_0\}}}. \tag{5}$$

Adding the signal and noise root power waves, the resulting root power wave incident on the load is denoted as $\mathsf{b}_{\mathsf{R}}(f)$ [20]. By replacing $\mathsf{a}_{\mathsf{T}}(f)$ with $\mathsf{b}_{\mathsf{RS}}(f)$ in (4), we obtain the received signal power spectral density $P_{\mathsf{RS}}(f)$. Similarly, by replacing $\mathsf{a}_{\mathsf{T}}(f)$ with $\mathsf{b}_{\mathsf{RN}}(f)$ in (4), we obtain the received noise spectral density $P_{\mathsf{RN}}(f)$. Let k_B be the Boltzmann constant in J/K and T be temperature in K. We set $P_{\mathsf{RN}}(f) = \mathsf{N}_0 = k_B T \left[\frac{\mathrm{W}}{\mathrm{Hz}}\right]$. At the receiver, we define

$$\mathsf{SNR}(f) = \frac{P_{\mathsf{RS}}(f)}{\mathsf{N}_0}. \tag{6}$$

The $\mathsf{SNR}(f)$ is non-zero in the band for which $P_{\mathsf{T}}(f)$ is non-zero.

Assuming Gaussian channel noise, the mutual information per unit time (bits/s) between the transmit and received Gaussian random process is

$$\mathsf{MI} = \int_{-\infty}^{\infty} \frac{1}{2} \log_2(1 + \mathsf{SNR}(f)) \mathrm{d}f. \tag{7}$$

For a real-valued passband signal, $\mathsf{SNR}(f)$ is symmetric about $f = 0$. This simplifies the definition to an integral over positive frequencies as

$$\mathsf{MI} = \int_{0}^{\infty} \log_2(1 + \mathsf{SNR}(f)) \mathrm{d}f. \tag{8}$$

Although integration upper limit is unbounded, SNR is positive only for a specific frequency range corresponding to the signal bandwidth which results in a finite integral value. In Section II-C, we describe the model of a MISO communication system and define $\mathsf{SNR}(f)$ in terms of $P_{\mathsf{T}}(f)$ and the scattering parameters of the individual linear sub-networks.

C. Circuit model of a MISO communication system in terms of scattering parameters

We analyze the achievable rate of a MISO wireless system consisting of a transmit array with N antennas and a single receive antenna. The transmitter hardware consists of a single RF chain connected to N antennas through an impedance-matching network and an analog beamforming network. The proposed model is applicable to any general type of antenna, array, analog beamformer, and matching network. In this paper, we focus on the design of transmit matching network.

The circuit theoretic model of the MISO communication system is shown in Fig. 2(b). The transmit array with N antennas and the single receive antenna form an $(N + 1)$ port network. Let $\mathbf{S}_{\mathsf{T}}(f) \in \mathbb{C}^{N \times N}$ be the scattering parameter matrix for the transmit array and $\mathsf{S}_{\mathsf{R}}(f) \in \mathbb{C}$ be the scattering parameter of the receive antenna. The wireless propagation channel scattering parameter is $\mathbf{s}_{\mathsf{RT}}^T(f) \in \mathbb{C}^{1 \times N}$, which accounts for the antenna gains and frequency-selective fading between receiver and transmitter. The dependence of $\mathbf{s}_{\mathsf{RT}}^T(f)$ on parameters like the number of channel paths, large-scale, and small-scale fading is described in (41). Similarly, $\mathbf{s}_{\mathsf{TR}}(f) \in \mathbb{C}^{N \times 1}$ [17]. We assume that the transmit array is sufficiently far from the receive antenna such that the signal attenuation between them is large [17], [20]. Hence, we can use the unilateral approximation by setting $\mathbf{s}_{\mathsf{TR}}(f) = \mathbf{0}_{N \times 1}$, i.e., we assume that the transmitter is unaffected by the electromagnetic fields at the receiver. The $(N+1)$ port network block scattering parameter matrix is defined and simplified as

$$\mathbf{S}_{\mathsf{H}}(f) = \begin{bmatrix} \mathbf{S}_{\mathsf{T}}(f) & \mathbf{s}_{\mathsf{TR}}(f) \\ \mathbf{s}_{\mathsf{RT}}^T(f) & \mathsf{S}_{\mathsf{R}}(f) \end{bmatrix} = \begin{bmatrix} \mathbf{S}_{\mathsf{T}}(f) & \mathbf{0}_{N \times 1} \\ \mathbf{s}_{\mathsf{RT}}^T(f) & \mathsf{S}_{\mathsf{R}}(f) \end{bmatrix}. \tag{9}$$

The incident root power wave vector on the transmit antenna array is denoted as $\mathbf{a}_{\mathsf{A}}(f) \in \mathbb{C}^{N \times 1}$ and the reflected root power wave vector is $\mathbf{b}_{\mathsf{A}}(f) \in \mathbb{C}^{N \times 1}$, as shown in Fig. 2(b). The root power wave vectors at the receiver and transmitter ports are related using $\mathbf{S}_{\mathsf{H}}(f)$ as

$$[\mathbf{b}_{\mathsf{A}}^T(f), \mathsf{b}_{\mathsf{RS}}(f)]^T = \mathbf{S}_{\mathsf{H}}(f)[\mathbf{a}_{\mathsf{A}}^T(f), 0]^T. \tag{10}$$

With the unilateral approximation, we can isolate the transmitter circuit model by writing

$$\mathbf{b}_{\mathsf{A}}(f) = \mathbf{S}_{\mathsf{T}}(f)\mathbf{a}_{\mathsf{A}}(f). \tag{11}$$

Using (9) and (10), the received signal root power wave is

$$\mathsf{b}_{\mathsf{RS}}(f) = \mathbf{s}_{\mathsf{RT}}^T(f)\mathbf{a}_{\mathsf{A}}(f). \tag{12}$$

The unilateral approximation enables simplification of the communication system analysis and design. It is also reasonable from a practical perspective because the signal attenuates heavily from transmitter to the receiver [17].

The transmitter network is characterized through the transmit impedance-matching network and analog beamforming network. The scattering parameter matrix of the analog beamforming network is denoted as the $(N+1) \times (N+1)$ complex matrix

$$\mathbf{S}_{\mathsf{F}}(f) = \begin{bmatrix} \mathsf{S}_{\mathsf{F},11}(f) & \mathbf{s}_{\mathsf{F},12}^T(f) \\ \mathbf{s}_{\mathsf{F},21}(f) & \mathbf{S}_{\mathsf{F},22}(f) \end{bmatrix}, \tag{13}$$

where $\mathsf{S}_{\mathsf{F},11}(f) \in \mathbb{C}$, $\mathbf{s}_{\mathsf{F},12}^T(f) \in \mathbb{C}^{1 \times N}$, $\mathbf{s}_{\mathsf{F},21}(f) \in \mathbb{C}^{N \times 1}$, and $\mathbf{S}_{\mathsf{F},22}(f) \in \mathbb{C}^{N \times N}$. The combination of the antenna array and the analog beamforming network can be treated as an equivalent load with scattering parameter denoted as $\mathsf{S}_{\mathsf{eq}}(f)$. We express $\mathsf{S}_{\mathsf{eq}}(f)$ in terms of the scattering parameter matrix elements of the array and the analog network as [2]

$$\begin{aligned} \mathsf{S}_{\mathsf{eq}}(f) = \mathsf{S}_{\mathsf{F},11}(f) + \mathbf{s}_{\mathsf{F},12}^T(f)\mathbf{S}_{\mathsf{T}}(f) \\ \times (\mathbf{I} - \mathbf{S}_{\mathsf{F},22}(f)\mathbf{S}_{\mathsf{T}}(f))^{-1}\mathbf{s}_{\mathsf{F},21}(f). \end{aligned} \tag{14}$$

The scattering parameter matrix of the transmit impedance-matching network, which connects the transmit source to the equivalent load, is denoted as

$$\mathbf{S}_{\mathsf{M}}(f) = \begin{bmatrix} \mathsf{S}_{\mathsf{M},11}(f) & \mathsf{S}_{\mathsf{M},12}(f) \\ \mathsf{S}_{\mathsf{M},21}(f) & \mathsf{S}_{\mathsf{M},22}(f) \end{bmatrix}. \tag{15}$$

For the single antenna case, the transmitter network only consists of the matching network. As there is no analog beamformer for the single antenna, the scattering parameter of the equivalent load is the scattering parameter of the antenna, i.e., $\mathsf{S}_{\mathsf{eq}}(f) = \mathsf{S}_{\mathsf{T}}(f)$.

To establish a linear relationship between the received signal root power wave $\mathsf{b}_{\mathsf{RS}}(f)$ and the transmit signal root power wave $\mathsf{a}_{\mathsf{T}}(f)$, we apply the scattering parameter definition for each block shown in Fig. 2(b). Let the incident root power wave on the combined load of antennas and analog beamforming network be denoted as $\mathsf{a}_{\mathsf{F}}(f)$. The reflected root power wave from the combined load is

$$\mathsf{b}_{\mathsf{F}}(f) = \mathsf{S}_{\mathsf{eq}}(f)\mathsf{a}_{\mathsf{F}}(f). \tag{16}$$

We express $\mathbf{a}_{\mathsf{A}}(f)$ in terms of $\mathsf{a}_{\mathsf{F}}(f)$ using the scattering parameter matrix elements as

$$\mathbf{a}_{\mathsf{A}}(f) = (\mathbf{I} - \mathbf{S}_{\mathsf{F},22}(f)\mathbf{S}_{\mathsf{T}}(f))^{-1}\mathbf{s}_{\mathsf{F},21}(f)\mathsf{a}_{\mathsf{F}}(f). \tag{17}$$

Finally, $\mathsf{a}_{\mathsf{F}}(f)$ is expressed in terms of the incident root power wave on the transmit impedance-matching network

$$\mathsf{a}_{\mathsf{F}}(f) = \frac{\mathsf{S}_{\mathsf{M},21}(f)}{1 - \mathsf{S}_{\mathsf{M},22}(f)\mathsf{S}_{\mathsf{eq}}(f)}\mathsf{a}_{\mathsf{T}}(f). \tag{18}$$

Using (12), (14), (17), (18), we relate $\mathsf{b}_{\mathsf{RS}}(f)$ to $\mathsf{a}_{\mathsf{T}}(f)$ using a channel coefficient corresponding to an equivalent SISO channel

$$H_{\mathsf{SISO}}(f) = \frac{\mathbf{s}_{\mathsf{RT}}^{T}(f)(\mathbf{I} - \mathbf{S}_{\mathsf{F},22}(f)\mathbf{S}_{\mathsf{T}}(f))^{-1}\mathbf{s}_{\mathsf{F},21}(f)\mathsf{S}_{\mathsf{M},21}(f)}{1 - \mathsf{S}_{\mathsf{M},22}(f)\mathsf{S}_{\mathsf{eq}}(f)}. \tag{19}$$

Hence, we have $\mathsf{b}_{\mathsf{RS}}(f) = H_{\mathsf{SISO}}(f)\mathsf{a}_{\mathsf{T}}(f)$. The equivalent channel in (19) depends not only on the wireless propagation channel but also captures the frequency-selectivity effect of antennas and matching network.

The equivalent channel expression is used for relating the received signal power spectral density to that available from the transmitter side. Using (19) and the definition of the power spectral density in (4), we relate $P_{\mathsf{RS}}(f)$ to $P_{\mathsf{T}}(f)$ as

$$P_{\mathsf{RS}}(f) = |H_{\mathsf{SISO}}(f)|^2 P_{\mathsf{T}}(f) \left[\frac{\mathrm{W}}{\mathrm{Hz}}\right]. \tag{20}$$

The $\mathsf{SNR}(f)$ in terms of $P_{\mathsf{T}}(f)$ and the equivalent channel is

$$\mathsf{SNR}(f) = |H_{\mathsf{SISO}}(f)|^2 \frac{P_{\mathsf{T}}(f)}{\mathsf{N}_0}. \tag{21}$$

The mutual information per unit time is $\int_0^\infty \log_2\left(1 + |H_{\mathsf{SISO}}(f)|^2 \frac{P_{\mathsf{T}}(f)}{\mathsf{N}_0}\right) \mathrm{d}f$. It depends on the design of the matching network and the transmit power allocation at each frequency. We assume a bandlimited source that supplies a maximum power per frequency $\mathsf{E}_{\mathsf{s}}\left[\frac{\mathrm{W}}{\mathrm{Hz}}\right]$ for $f \in [f_{\mathsf{min}}, f_{\mathsf{max}}]$ [22]. For the bandwidth $B = f_{\mathsf{max}} - f_{\mathsf{min}}$, we assumed a fixed total supplied power $B\mathsf{E}_{\mathsf{s}}\mathrm{W}$. Assuming that the source supplies the maximum available power at each frequency, we define the achievable rate in bits/s as

$$\mathsf{R} = \int_{f_{\mathsf{min}}}^{f_{\mathsf{max}}} \log_2\left(1 + |H_{\mathsf{SISO}}(f)|^2 \frac{\mathsf{E}_{\mathsf{s}}}{\mathsf{N}_0}\right) \mathrm{d}f. \tag{22}$$

In Section III, we optimize the achievable rate R by optimally designing the matching network.

III. Optimizing achievable rate under Bode-Fano matching constraints

In this section, we propose a general framework for optimizing the achievable rate as a function of the matching network. The rate depends on the matching network through the term $H_{\mathsf{SISO}}(f)$ as shown in (19) which depends on the matching network scattering parameter matrix elements $\mathsf{S}_{\mathsf{M},21}(f)$ and $\mathsf{S}_{\mathsf{M},22}(f)$. The values for these elements at each frequency are hardware specific, i.e., dependent on the actual physical elements like the inductors and capacitors used for building the matching network circuit. One approach of optimizing rate is to define the rate objective in terms of the physical component values for a fixed structure [4]. A limitation of this approach is that it does not guarantee that the specific circuit gives better performance theoretically than any other physically realizable matching network. In this paper, instead of optimizing the rate in terms of the physical components of a specific matching circuit, we formulate and solve a general problem that applies to any matching network made of passive and linear elements. In Section III-A, we describe the constraints associated with any general passive matching network.

A. General form of the Bode-Fano matching constraint

The first systematic approach to study the bandwidth limitation of a matching network was proposed by Bode for a special type of reactive load [8]. The work by Bode was generalized by Fano for arbitrary reactive loads [9]. These results on the bandwidth limitation of matching networks are popularly known as Bode-Fano limits [5]. Recently, a generalization of the Bode-Fano matching limits was proposed for arbitrary loads like an antenna array with an analog beamforming network [2], [31]. We use these results from [2], [31] to formulate the matching network constraints in the achievable rate optimization problem.

The Bode-Fano constraints place a bound on the power loss ratio metric [2]. The constraints are expressed in terms of the power loss ratio, which indicates the ratio of expected power lost (due to reflection and dissipation) to the expected input power where the expectation is over the input random signal. Mathematically, it is given as

$$\begin{aligned} r^2(f) &= 1 - \frac{\mathbb{E}[|\mathsf{a}_{\mathsf{F}}(f)|^2 - |\mathsf{b}_{\mathsf{F}}(f)|^2]}{\mathbb{E}[|\mathsf{a}_{\mathsf{T}}(f)|^2]} \\ &\overset{(a)}{=} 1 - \frac{|\mathsf{S}_{\mathsf{M},21}(f)|^2}{|1 - \mathsf{S}_{\mathsf{M},22}(f)\mathsf{S}_{\mathsf{eq}}(f)|^2}(1 - |\mathsf{S}_{\mathsf{eq}}(f)|^2), \end{aligned} \tag{23}$$

where equality (a) follows from the definition of $\mathsf{b}_{\mathsf{F}}(f)$ and (18). We also define the transmission coefficient as

$$\mathcal{T}(f) = 1 - r^2(f). \tag{24}$$

A lower value of $r^2(f)$ or a higher value of $\mathcal{T}(f)$ for a specified bandwidth indicates a better power transfer to the equivalent load in the desired band.

Cauchy's integral relations in complex variable calculus can be applied to any linear circuit model for deriving Bode-Fano constraints [9]. Mathematically, it is convenient to analyze the circuit model as a function of the complex frequency $s = \sigma + \mathrm{j}2\pi f$ [9] [31]. Similar to the original Bode-Fano constraints, we assume that the load should be realizable by means of finite passive lumped elements [9]. Therefore, we use a rational approximation of $\mathsf{S}_{\mathsf{eq}}(f)$ defined in the whole complex plane and denoted as $\hat{\mathsf{S}}_{\mathsf{eq}}(s)$ [31]. We assume that $\hat{\mathsf{S}}_{\mathsf{eq}}(s)$ should be in the rational form and satisfy the passivity condition [31]. The guidelines for obtaining $\hat{\mathsf{S}}_{\mathsf{eq}}(s)$ from $\mathsf{S}_{\mathsf{eq}}(f)$ are discussed in detail in [31]. Note that $\hat{\mathsf{S}}_{\mathsf{eq}}(s)$ is not unique and depends on the technique used to approximate $\mathsf{S}_{\mathsf{eq}}(f)$. We briefly summarize the approximation techniques from [31] in Appendix A.

The Bode-Fano theory provides a set of constraints on the power loss ratio $r^2(f)$ for any passive and linear impedance-matching network terminated with a passive load realized using lumped elements. These constraints are expressed as bounds on the integral of logarithm of the power loss ratio [2], [9], [15]. For a simple load of resistor R and capacitor C in parallel, there is only one Bode-Fano constraint expressed as [5]

$$\int_0^\infty \log\left(\frac{1}{r^2(f)}\right) \mathrm{d}f \leq \frac{1}{RC}. \tag{25}$$

For an arbitrary load, the number of necessary constraints for the physical realizability of $r^2(f)$ is determined using

a Darlington equivalent representation of the load. From Darlington's theory, any physically realizable impedance is equivalent to the input impedance of a reactive two-port network terminated with a 1Ω resistor [40]. The number of such necessary constraints on $r^2(f)$ equals the number of independent parameters used to define the Darlington equivalent network of the load [9]. For example, for a load of resistor, inductor, and capacitor in series, the Darlington equivalent is specified using the quality factor value and the resonant frequency which results in two Bode-Fano bounds [15, Eq 11].

For an equivalent load with rational approximation $\hat{\mathsf{S}}_{\mathsf{eq}}(s)$, we assume there are N_{BF} number of distinct constraints for describing the physical realizability of the power loss ratio. For the ith constraint where $i \in \{1, 2, \ldots, N_{\mathsf{BF}}\}$, we define two positive terms $\xi_{\mathsf{BF},i}(f)$ and $B_{\mathsf{BF},i}$. The term $\xi_{\mathsf{BF},i}(f)$ is a prelog term in the integrand which is multiplied by the logarithm of the power loss ratio. The term $B_{\mathsf{BF},i}$ is an upper bound on the Bode-Fano integral. For a load whose scattering parameter after rational approximation is $\hat{\mathsf{S}}_{\mathsf{eq}}(s)$, the N_{BF} distinct constraints required for the realizability of power loss ratio $r^2(f)$ are [2]

$$\int_0^\infty \xi_{\mathsf{BF},i}(f) \log\left(\frac{1}{r^2(f)}\right) \mathrm{d}f \leq B_{\mathsf{BF},i}, \text{for } \{i\}_1^{N_{\mathsf{BF}}}, \quad (26)$$

where $\xi_{\mathsf{BF},i}(f)$ and $B_{\mathsf{BF},i}$ are positive terms evaluated using $\hat{\mathsf{S}}_{\mathsf{eq}}(s)$ as discussed in Appendix B. The value of N_{BF}, in general, equals the number of unique non-repeating solutions to (50) in Appendix B. In case of repeating solutions, the maximum value of N_{BF} equals the multiplicity of the root [31]. The detailed proof of the general form of the Bode-Fano constraint is given in [31].

In Section III-B, we will use the constraints defined in (26) for formulating the achievable rate optimization problem as a function of the transmission coefficient $\mathcal{T}(f)$ defined in (24). Before proceeding to the problem formulation, we first rewrite the achievable rate in terms of the transmission coefficient so that both constraints and objective in the optimization can be expressed as function of the variable $\mathcal{T}(f)$.

B. Achievable rate optimization problem formulation

The achievable rate metric depends on the matching network through the scattering parameters $\mathsf{S}_{\mathsf{M},21}(f)$ and $\mathsf{S}_{\mathsf{M},22}(f)$ as shown through (19) and (22). Using (19), (21), (23), and (24), we express $\mathsf{SNR}(f)$ in terms of $\mathcal{T}(f)$ as

$$\mathsf{SNR}(f) = |\mathbf{s}_{\mathsf{RT}}^T(f)(\mathbf{I} - \mathbf{S}_{\mathsf{F},22}(f)\mathbf{S}_{\mathsf{T}}(f))^{-1}\mathbf{s}_{\mathsf{F},21}(f)|^2 \times \frac{P_{\mathsf{T}}(f)\mathcal{T}(f)}{(1-|\mathsf{S}_{\mathsf{eq}}(f)|^2)\mathsf{N}_0}. \quad (27)$$

From (27), the achievable rate expression is

$$\mathsf{R} = \int_{f_{\mathsf{min}}}^{f_{\mathsf{max}}} \log_2\left(1 + \frac{|\mathbf{s}_{\mathsf{RT}}^T(f)(\mathbf{I} - \mathbf{S}_{\mathsf{F},22}(f)\mathbf{S}_{\mathsf{T}}(f))^{-1}\mathbf{s}_{\mathsf{F},21}(f)|^2}{(1-|\mathsf{S}_{\mathsf{eq}}(f)|^2)} \times \frac{\mathsf{E}_{\mathsf{s}}}{\mathsf{N}_0}\mathcal{T}(f)\right)\mathrm{d}f. \quad (28)$$

In the ideal matching network case, i.e., no power loss due to reflection or dissipation, $\mathcal{T}(f) = 1$, and the ideal lossless SNR is expressed as

$$\mathsf{SNR}_{\text{ideal}}(f) = \frac{|\mathbf{s}_{\mathsf{RT}}^T(f)(\mathbf{I} - \mathbf{S}_{\mathsf{F},22}(f)\mathbf{S}_{\mathsf{T}}(f))^{-1}\mathbf{s}_{\mathsf{F},21}(f)|^2}{(1-|\mathsf{S}_{\mathsf{eq}}(f)|^2)} \frac{\mathsf{E}_{\mathsf{s}}}{\mathsf{N}_0}. \quad (29)$$

The achievable rate for the ideal case is

$$\mathsf{R}_{\text{ideal}} = \int_{f_{\mathsf{min}}}^{f_{\mathsf{max}}} \log_2\left(1 + \mathsf{SNR}_{\text{ideal}}(f)\right) \mathrm{d}f. \quad (30)$$

The ideal SNR depends on the wireless propagation channel, the scattering parameters of the antenna array, and the analog beamforming network but does not depend on the matching network. For a physically realizable matching network, $\mathcal{T}(f) \leq 1$. Therefore, $\mathsf{R} \leq \mathsf{R}_{\text{ideal}}$ meaning that the achievable rate is over-estimated when Bode-Fano constraints are disregarded.

We formulate the achievable rate optimization problem to optimally design the transmission coefficient $\mathcal{T}(f)$. In (28), we defined the optimization objective in terms of $\mathcal{T}(f)$. Similarly, the Bode-Fano inequalities from (26) can be expressed in terms of $\mathcal{T}(f)$ using (24). The achievable rate optimization problem in terms of $\mathcal{T}(f)$ using (26), (28), and (29) is

$$\mathsf{R}_{\max} = \max_{\mathcal{T}(f)} \int_{f_{\mathsf{min}}}^{f_{\mathsf{max}}} \log_2(1 + \mathsf{SNR}_{\text{ideal}}(f)\mathcal{T}(f))\mathrm{d}f, \quad (31a)$$

$$\text{s.t.} \int_0^\infty \xi_{\mathsf{BF},i}(f) \log\left(\frac{1}{1-\mathcal{T}(f)}\right) \mathrm{d}f \leq B_{\mathsf{BF},i}, \text{for } \{i\}_1^{N_{\mathsf{BF}}} \quad (31b)$$

$$0 \leq \mathcal{T}(f) \leq 1. \quad (31c)$$

The constraint in (31c) follows from the definition of the transmission coefficient in (24). Comparing this formulation to [22], the key difference is that $\mathcal{T}(f)$ was defined on the receiver side between a single antenna and the low-noise amplifier in [22]. This led to $\mathcal{T}(f)$ appearing in both signal power and the extrinsic noise power in [22, Eq 21]. The problem formulation in our work expressed in (31) uses the $\mathcal{T}(f)$ defined between the transmit RF chain and the equivalent load of multiple transmit antennas and analog beamforming network. So $\mathcal{T}(f)$ appears only in the signal power leading to an optimal solution expression different from [22, Eq 25].

C. Optimal transmission coefficient

We use the Lagrangian to solve the optimization problem in (31). The total number of constraints in (31b) and (31c) is $N_{\mathsf{BF}} + 2$. For the ith constraint, we denote the Lagrangian parameter as μ_i. The Lagrangian is [41]

$$\mathcal{L}\left(\mathcal{T}(f), \mu_i|_{i=1}^{N_{\mathsf{BF}}+2}\right) = -\int_{f_{\mathsf{min}}}^{f_{\mathsf{max}}} \log_2(1 + \mathsf{SNR}_{\text{ideal}}(f)\mathcal{T}(f))\mathrm{d}f + \sum_{i=1}^{N_{\mathsf{BF}}} \mu_i \left(\int_0^\infty \xi_{\mathsf{BF},i}(f) \log\left(\frac{1}{1-\mathcal{T}(f)}\right) \mathrm{d}f - B_{\mathsf{BF},i}\right) - \mu_{N_{\mathsf{BF}}+1}\mathcal{T}(f) + \mu_{N_{\mathsf{BF}}+2}(\mathcal{T}(f) - 1). \quad (32)$$

The solution to (31) is obtained after applying *Karush-Kuhn-Tucker* (KKT) conditions in Appendix C [22]. The maximum

rate is defined in terms of the optimal transmission coefficient $\mathcal{T}^\star(f)$ as

$$\mathsf{R}_{\max} = \int_{f_{\min}}^{f_{\max}} \log_2(1 + \mathsf{SNR}_{\text{ideal}}(f)\mathcal{T}^\star(f))\mathrm{d}f. \tag{33}$$

The expression for $\mathcal{T}^\star(f)$ is in terms of the optimal Lagrangian parameters $\mu_i^\star|_{i=1}^{N_{\mathsf{BF}}}$ described as follows.

Theorem 1: The relationship between the variables $\mathcal{T}^\star(f)$ and $\mu_i^\star|_{i=1}^{N_{\mathsf{BF}}}$ corresponding to the optimal solution of the optimization problem in (31) is as follows.

$$\mathcal{T}^\star(f) = \left[\frac{1 - \ln 2 \frac{\sum_{i=1}^{N_{\mathsf{BF}}} \mu_i^\star \xi_{\mathsf{BF},i}(f)}{\mathsf{SNR}_{\text{ideal}}(f)}}{1 + \ln 2 \sum_{i=1}^{N_{\mathsf{BF}}} \mu_i^\star \xi_{\mathsf{BF},i}(f)}\right]^+, \quad \mu_i^\star|_{i=1}^{N_{\mathsf{BF}}} \geq 0, \tag{34a}$$

$$\mu_i^\star \left(\int_0^\infty \xi_{\mathsf{BF},i}(f) \log\left(\frac{1}{1 - \mathcal{T}^\star(f)}\right) \mathrm{d}f - B_{\mathsf{BF},i}\right) = 0, \{i\}_1^{N_{\mathsf{BF}}}, \tag{34b}$$

$$\left(\int_0^\infty \xi_{\mathsf{BF},i}(f) \log\left(\frac{1}{1 - \mathcal{T}^\star(f)}\right) \mathrm{d}f - B_{\mathsf{BF},i}\right) \leq 0, \{i\}_1^{N_{\mathsf{BF}}}. \tag{34c}$$

Proof: Refer to Appendix C for proof. □

The expression for the optimal transmission coefficient computed using (34) can be interpreted as waterfilling in the frequency domain which is a fundamental result by Shannon in information theory [42]. From (34a), we observe that $\mathcal{T}^\star(f)$ is higher for frequencies with better $\mathsf{SNR}_{\text{ideal}}(f)$. As $\mathsf{SNR}_{\text{ideal}}(f)$ is inversely proportional to bandwidth, the peak gain in $\mathcal{T}^\star(f)$ for higher bandwidths is lower and vice versa. This shows that the fundamental gain-bandwidth tradeoff of matching networks is captured in the expression of $\mathcal{T}^\star(f)$ in (34a).

The solution approach to derive the optimal transmission coefficient is different from the classical waterfilling problem. The classical [7] and generalized version of the waterfilling problem [43] involve summation over discrete terms unlike the formulation in our work which involves a continuous function of frequency. We leverage variational calculus in Appendix C to derive the optimal transmission coefficient. Due to the numerical integration in constraints, it is difficult to apply the algorithm from classical and generalized waterfilling based on discrete power allocation [43]. Moreover, the variables $\mathcal{T}^\star(f)$ and $\mu_i^\star|_{i=1}^{N_{\mathsf{BF}}}$ corresponding to the optimal solution of the optimization problem in (31) are tightly coupled in the equations (34a), (34b), and (34c). We use a numerical approach to compute a sub-optimal solution. We set all but one Lagrangian parameters to 0, apply a bisection search on the non-zero parameter till (34b) is satisfied within a threshold, and repeat this process for all parameters to obtain the values of $\mu_i^\star|_{i=1}^{N_{\mathsf{BF}}}$ that maximize the rate. This low-complexity numerical approach ensures that (34b) is satisfied for $N_{\mathsf{BF}} - 1$ parameters and within a specific tolerance for one parameter. The approximate solution for $\mathcal{T}^\star(f)$ is obtained by substituting the optimized values of $\mu_i^\star|_{i=1}^{N_{\mathsf{BF}}}$ in (34a).

All passive and linear matching networks will provide an achievable rate less than the value of $\mathsf{R}_{\max}$. This maximum achievable rate based on Bode-Fano bounds is more accurate than $\mathsf{R}_{\text{ideal}}$ which disregards the matching theory. This rate $\mathsf{R}_{\max}$ is a new benchmark for designing matching networks instead of a metric like power transfer efficiency which does not capture the effect of wireless propagation channel.

IV. Matching network circuit design methodology and illustrations

From a system design perspective, it is crucial to provide a practical methodology to approximate the theoretical achievable rate bound from Section III. In this section, we address the second question, "How to design impedance-matching networks to approximate this achievable rate bound?" We propose a practical matching network design approach using $\mathcal{T}^\star(f)$ from (34a).

A. General methodology to design matching network

We provide a three step procedure to design a matching network based on the achievable rate upper bound as follows.

1) **Evaluation of Bode-Fano constraints**
   a) For a given scattering matrix of an antenna $\mathbf{S}_{\mathsf{T}}(f)$ and analog beamforming network $\mathbf{S}_{\mathsf{F}}(f)$, obtain a passive rational approximation as a function of the complex frequency to evaluate the rational function of the scalar equivalent load $\hat{\mathsf{S}}_{\mathsf{eq}}(s)$.
   b) Evaluate N_{BF} Bode-Fano constraints using the expression of $\hat{\mathsf{S}}_{\mathsf{eq}}(s)$ based on Table I in Appendix B.
2) **Optimal transmission coefficient**
   a) Solve the optimization problem (31) for the N_{BF} Bode-Fano constraints by numerically solving the system of equations and inequalities given by (34).
   b) Compute $\mathcal{T}^\star(f)$ for the optimized $\mu_i^\star|_{i=1}^{N_{\mathsf{BF}}}$ using (34a).
3) **Approximating $\mathcal{T}^\star(f)$ with a practical matching network topology**
   a) Choose a general reactive ladder circuit with a fixed order.
   b) Optimize the component values of the matching network circuit topology to fit the desired frequency response of the optimal transmission coefficient $\mathcal{T}^\star(f)$.

In the first step, overfitting when approximating $\mathsf{S}_{\mathsf{eq}}(f)$ with $\hat{\mathsf{S}}_{\mathsf{eq}}(s)$ can result in loose Bode-Fano bounds. Sometimes, there exists poles and zeros in the rational approximation which are close to each other. As observed from expression of B_{BF} from Table I in Appendix B, overfitting may result in higher bounding values of B_{BF} [31]. Overfitting is an issue if the computed value of $\mathcal{T}^\star(f)$ is close to one even for higher bandwidths. The gain-bandwidth tradeoff will not be captured due to overfitting. This issue can be avoided by reducing the model order.

B. Application of matching network design methodology to a single Chu's antenna

We present numerical illustrations for the matching network design methodology. For simulations, we use Chu's antenna at receiver and transmitter, similar to [22], to provide generic

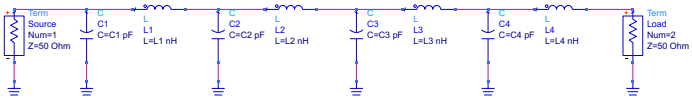

Fig. 3: Circuit model of the 4th order LC ladder in ADS software. This simple topology can be used to approximate the transmission coefficient response obtained from the optimization problem.

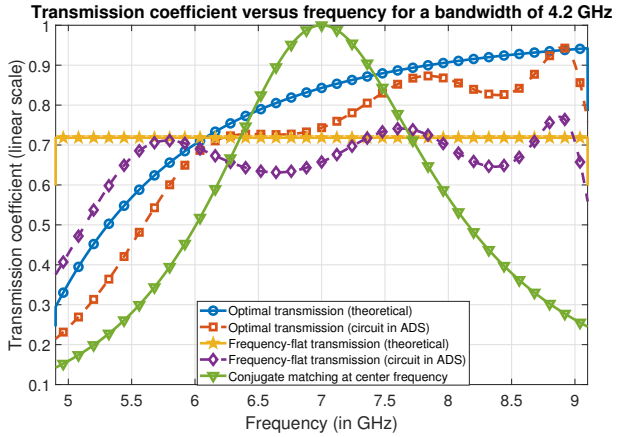

(a) Bandwidth of 4.2 GHz.

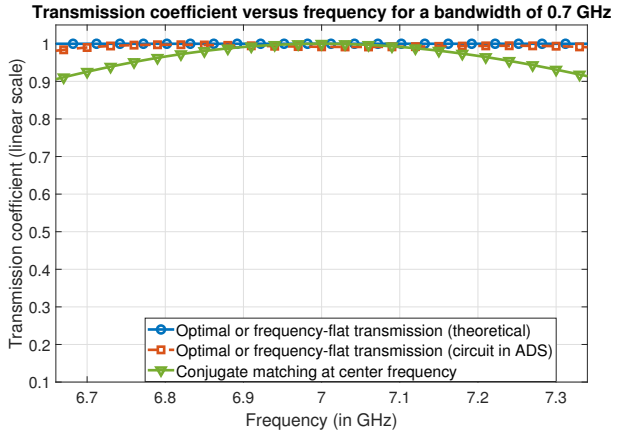

(b) Bandwidth of 0.7 GHz.

Fig. 4: For (a), the optimal transmission curve is higher than the frequency-flat transmission curve for frequencies greater than 6.1 GHz. For (b), the optimal transmission coincides with the frequency-flat transmission curves. Conjugate matching response is same for both bandwidths whereas the proposed optimal transmission and frequency-flat transmission responses change with the bandwidth.

insights without using a specific antenna design. Although Bode-Fano bounds depend on the antenna type, the achievable rate optimization methodology is general and can be applied to any antenna design.

Chu's antenna model: Let the Chu's antenna structure be enclosed in a spherical volume with radius a. Let the speed of light be denoted as c and characteristic resistance be denoted as R. The Chu's electric antenna is modeled with an equivalent circuit consisting of a capacitor $C = \frac{a}{cR}$ in series with a parallel combination of an inductor $L = \frac{aR}{c}$ and resistor R [22, Fig. 2]. The input impedance is

$$\mathsf{Z}_{\mathsf{T}}(f) = \mathsf{Z}_{\mathsf{R}}(f) = \frac{R}{\mathrm{j}2\pi f\frac{a}{c}} + \frac{R}{1+(\mathrm{j}2\pi f\frac{a}{c})^{-1}}. \tag{35}$$

The scattering parameter in rational form is

$$\hat{\mathsf{S}}_{\mathsf{T}}(s) = \frac{1}{(2s^2\frac{a^2}{c^2} + 2s\frac{a}{c} + 1)}. \tag{36}$$

For a single antenna, there is no analog beamforming network, hence, $\hat{\mathsf{S}}_{\mathsf{eq}}(s) = \hat{\mathsf{S}}_{\mathsf{T}}(s)$.

Bode-Fano bounds for a single Chu's antenna: Substituting $\hat{\mathsf{S}}_{\mathsf{eq}}(s)$ in (50), we obtain $s^4 = 0$. For repeated roots with multiplicity 4, we apply [31, Eq. 22] to derive the bounds

$$\int_0^\infty \frac{1}{2\pi^2 f^2}\log\left(\frac{1}{1-\mathcal{T}(f)}\right)\mathrm{d}f \le \frac{2a}{c}, \tag{37a}$$

$$\int_0^\infty \frac{1}{8\pi^4 f^4}\log\left(\frac{1}{1-\mathcal{T}(f)}\right)\mathrm{d}f \le \frac{4a^3}{3c^3}. \tag{37b}$$

The bounds are in the form specified in (31b) with $N_{\mathsf{BF}} = 2$.

Parameter setup: Let $f_{\mathsf{c}} = 7$ GHz. The corresponding wavelength $\lambda_{\mathsf{c}} = 4.29$ cm. Let $a = \frac{\lambda_{\mathsf{c}}}{10} = 4.29$ mm, bandwidth $B \in \{0.1f_{\mathsf{c}}, 0.6f_{\mathsf{c}}\} = \{0.7, 4.2\}$ GHz, $\mathsf{E_s} = \frac{0.25}{B}\left[\frac{\mathrm{W}}{\mathrm{Hz}}\right]$, and $R = 50\Omega$. Let the distance between receiver and transmitter be $d_{tx-rx} = 500$m and the antenna gain $G = 1.5$. The wireless channel is known at the transmitter and defined as [20]

$$\mathsf{S}_{\mathsf{RT}}(f) = \frac{1-\mathsf{S}_{\mathsf{T}}(f)}{\mathsf{Z}_0 + Z_{\mathsf{R}}(f)}\frac{c}{2\pi f d_{tx-rx}}G\mathcal{R}(Z_{\mathsf{T}}(f)). \tag{38}$$

Using $k_B = 1.38\times10^{-23}$ J/K and $T = 290K$, we get $\mathsf{N}_0 = 4\times10^{-21}\left[\frac{\mathrm{W}}{\mathrm{Hz}}\right]$.

Optimal transmission coefficient approximation with an LC ladder: We compute the optimal transmission coefficient by solving the achievable rate optimization problem using two Bode-Fano bounds in (37). To approximate this transmission coefficient, it suffices to use a simple 4th order LC ladder shown in Fig. 3. We use Keysight ADS which is a circuit simulation software for characterizing and optimizing RF systems. The built-in optimization tool of ADS is leveraged for our simulations. In ADS, we define 8 design variables, L_i and C_i for $\{i\}_1^4$, and set the optimization goal based on the optimal transmission coefficient. The output is the optimized values of L_i and C_i. The optimization tool in ADS provides the optimized values for the chosen design variables by minimizing the weighted mean squared error between the simulated data points and desired data points on the transmission coefficient curve [44]. The transmission coefficient corresponding to the optimized circuit is used as a comparison benchmark.

Frequency-flat transmission coefficient approximation with an LC ladder: For comparison with the box-car matching approach in [15], we assume frequency-flat transmission coefficient in a band spanning f_{min} to f_{max}, i.e., $\mathcal{T}(f) = \mathcal{T}_{\mathsf{ff}}$ for $f \in [f_{\mathsf{min}}, f_{\mathsf{max}}]$. The value of $\mathcal{T}_{\mathsf{ff}}$ should satisfy both (37a) and (37b). We define

$$r_1 = \exp\left(\frac{-2a/c}{\int_{f_{\mathsf{min}}}^{f_{\mathsf{max}}} 1/(2\pi^2 f^2)\mathrm{d}f}\right), \tag{39a}$$

$$r_2 = \exp\left(\frac{-4a^3/(3c^3)}{\int_{f_{\mathsf{min}}}^{f_{\mathsf{max}}} 1/(8\pi^4 f^4)\mathrm{d}f}\right). \tag{39b}$$

The value of $\mathcal{T}_{\mathsf{ff}}$ satisfying both constraints is $\mathcal{T}_{\mathsf{ff}} = 1 - \text{Max}\{r_1, r_2\}$. The frequency-flat transmission coefficient is approximated similarly using a 4th order LC ladder in ADS.

In Fig. 4, we plot the transmission coefficient versus frequency for the theoretical case and the 4th order LC ladder circuit in Fig. 3 optimized in ADS. We see that the circuit implemented in ADS provides a good approximation of the desired transmission coefficient in the bandwidth of interest. This shows that with a simple matching network topology, it is possible to approximate the transmission coefficient. We also show the conjugate matching transmission coefficient benchmark in Fig. 4 which remains the same irrespective of the bandwidth. The proposed optimal transmission coefficient curves are dependent on the bandwidth. In Fig. 4a, although conjugate matching transmission has higher $\mathcal{T}(f)$ than the optimal transmission for frequencies 6.5 GHz to 7.4 GHz, this is because the optimal transmission is optimized for a larger band from 4.9 GHz to 9.1 GHz. In Fig. 4b, the optimal transmission is optimized for 6.65 GHz to 7.35 GHz and is higher than fixed conjugate matching. We use these transmission coefficients in Section V to compute the SNR, achievable rate, and its comparison with other benchmarks.

C. Application of matching network design methodology to a generalized MISO system

In Section IV-B, the design methodology illustration was for a single Chu's antenna for which closed-form model was available. For any general antenna array, the closed-form impedance model is not available. In this section, we present numerical illustrations for the matching network design methodology applied to a generalized MISO system consisting of dipole antenna array generated using MATLAB Antenna Toolbox.

Dipole antenna array simulation setup: We assume an array of $N = 8$ strip dipole antennas in a single plane. The length of each dipole antenna is $\ell_{\mathsf{dip}} = \frac{\lambda_{\mathsf{c}}}{4}$ and the width is $w_{\mathsf{dip}} = 0.1\ell_{\mathsf{dip}}$. The inter-antenna spacing is $d = \frac{\lambda_{\mathsf{c}}}{2}$. The scattering parameter matrix $\mathbf{S}_{\mathsf{T}}(f)$ is generated using the function $\mathsf{sparameters}(\cdot)$ in MATLAB RF toolbox. The impedance parameter matrix is calculated using the $\mathsf{s2z}(\cdot)$ function in MATLAB.

Analog beamforming network model: For the scattering matrix of the analog beamforming network, we assume $\mathsf{S}_{\mathsf{F},11}(f) = 0$, $\mathbf{S}_{\mathsf{F},22}(f) = \mathbf{0}_2$, and $\mathbf{s}_{\mathsf{F},12}(f) = \mathbf{s}^T_{\mathsf{F},21}(f)$ represents the beamforming vector corresponding to an ideal frequency-flat phased array. We also assume no insertion loss.

From (19), we see that $H_{\mathsf{SISO}}(f)$ depends on the analog beamforming vector $\mathbf{s}_{\mathsf{F},21}(f)$. In practice, $\mathbf{s}_{\mathsf{F},21}(f)$ can also be designed. In this paper, the focus is on the design of matching networks. We consider a simple approach to design the analog beamforming vector which influences $H_{\mathsf{SISO}}(f)$. To avoid complicated analog beamforming designs, we use a 1-bit resolution phased array model, i.e., the phase at each antenna belongs to the set $\{-1, 1\}$. The optimal analog beamformer is chosen from this discrete set of feasible phase-shifts such that it maximizes $|\mathsf{SNR}_{\mathsf{ideal}}(f_{\mathsf{c}})|^2$.

Parameter setup: For $f_{\mathsf{c}} = 7$ GHz, let bandwidth $B = 0.6f_{\mathsf{c}} = 4.2$ GHz, and $\mathsf{E}_{\mathsf{s}} = \frac{0.25}{B}\left[\frac{\mathrm{W}}{\mathrm{Hz}}\right]$. The channel is based

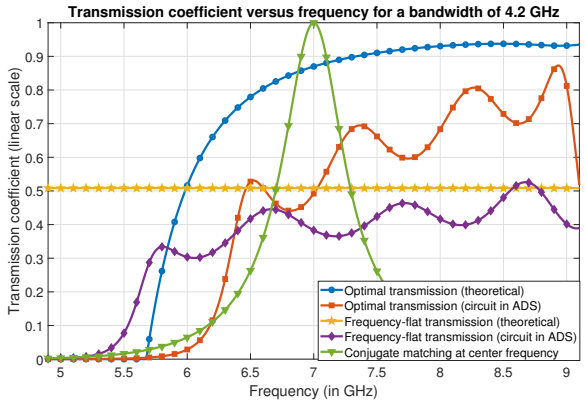

(a) Beamforming off-broadside at $\theta = \frac{\pi}{4}$

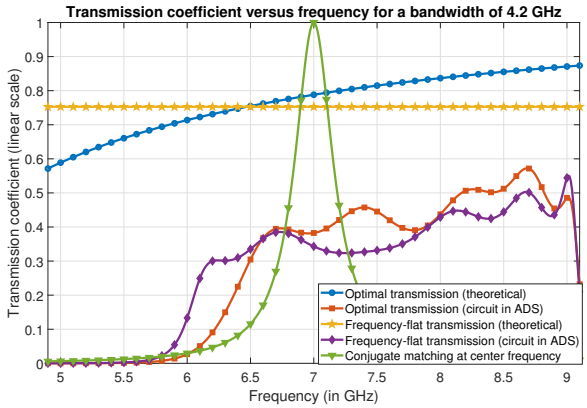

(b) Beamforming at broadside, i.e., $\theta = 0$

Fig. 5: For an array of $N = 8$ dipole antennas, the optimal transmission curves are higher than the frequency-flat transmission curves for a major portion of the bandwidth. As matching network order is fixed for both beamforming modes, the gap between theoretical and circuit response is different.

on the geometric frequency-selective multipath model with one dominant line-of-sight surrounded by several non-line-of-sight paths in a small angular spread. Let the line-of-sight path be at angle θ from broadside. We provide simulation for two cases: broadside beamforming, i.e., $\theta = 0$ and off-broadside beamforming with $\theta = \frac{\pi}{4}$. We model the multipath scattering with $L = 8$ non-line-of-sight paths at $\theta_\ell \sim \mathcal{U}(\theta - \frac{\pi}{20}, \theta + \frac{\pi}{20})$ and amplitude $\alpha_\ell \sim \mathcal{CN}(0, 1)$. The frequency selective array steering vector is

$$\mathbf{a}(\theta) = \left[1, \ldots, \exp\left(\mathrm{j}2\pi f \frac{(N-1)d\sin(\theta)}{c}\right)\right]^T. \tag{40}$$

The wireless multipath channel scattering parameter is [20]

$$\mathbf{s}_{\mathsf{RT}}(f) = \frac{cG\mathcal{R}(\mathsf{Z}_{\mathsf{T}}(f))(\mathbf{I}_2 - \mathbf{S}_{\mathsf{T}}(f))(\mathbf{a}(\theta) + \sum_{\ell=1}^{L}\alpha_\ell \mathbf{a}(\theta_\ell))}{2\pi f d_{tx-rx}(\mathsf{Z}_0 + \mathsf{Z}_{\mathsf{R}}(f))}. \tag{41}$$

In (41), the mutual coupling effect between antennas is captured through the dependence on $\mathbf{S}_{\mathsf{T}}(f)$.

Bode-Fano bounds for dipole antenna array: For both cases, we compute $\hat{\mathsf{S}}_{\mathsf{eq}}(s)$ and substitute it in (50) to solve for s. We obtain three unique roots with $\mathcal{R}(s_0) > 0$ which correspond to three Bode-Fano inequalities computed using

Table I in Appendix B. Through simulations, we observed that the value of N_{BF} does not significantly change for more number of antenna elements in the array. However, it may vary across different antenna types. The work on investigating the dependence of N_{BF} on factors like antenna type, mutual coupling between elements, and analog beamforming is a direction for future work.

Optimal transmission coefficient approximation with an LC ladder: We compute the optimal transmission coefficient by solving the achievable rate optimization problem using three Bode-Fano constraints. For approximating $\mathcal{T}^{\star}(f)$, it suffices to choose a 7th order LC ladder. In ADS, we define 14 design variables: L_i and C_i for $\{i\}_1^7$ and set the optimization goal based on $\mathcal{T}^{\star}(f)$. Note that the choice of model order can be changed depending on other design requirements.

Frequency-flat transmission coefficient approximation with an LC ladder: For comparison with the box-car matching approach in [15], let $\mathcal{T}_{\mathsf{ff}}$ satisfy all Bode-Fano constraints. Using Table I in Appendix B, for $\{i\}_1^3$, we define

$$r_i = \exp\left(\frac{\log\left(\left|\hat{\mathsf{S}}_{\mathsf{eq}}(s_i)\frac{\prod_{\ell=1}^{N_{\mathsf{z}}}(s_i+z_{\mathsf{eq},\ell})}{\prod_{\ell=1}^{N_{\mathsf{z}}}(s_i-z_{\mathsf{eq},\ell})}\right|\right)}{\int_{f_{\min}}^{f_{\max}}\mathcal{R}\{(s_i-\mathrm{j}2\pi f)^{-1}+(s_i+\mathrm{j}2\pi f)^{-1}\}\mathrm{d}f}\right). \tag{42}$$

The value of $\mathcal{T}_{\mathsf{ff}}$ satisfying both constraints is $\mathcal{T}_{\mathsf{ff}} = 1 - \mathrm{Max}\{r_1, r_2, r_3\}$. The frequency-flat transmission coefficient can be approximated similarly using a 7th order LC ladder in ADS.

In Fig. 5, we plot the transmission coefficient versus frequency for the theoretical case and the 7th order LC ladder circuit optimized in ADS. We observe that for a major portion of the 4.2 GHz bandwidth for both beamforming angles, optimal transmission response is higher than frequency-flat transmission response. This leads to a higher SNR and achievable rate.

V. SNR AND ACHIEVABLE RATE SIMULATIONS

In this section, we present the results for SNR and achievable rate corresponding to the following seven cases.

Upper bound (Shannon): This bound corresponds to the case when the Bode-Fano constraints are ignored, i.e., $\mathcal{T}(f) = 1 \forall f$. The ideal SNR denoted as $\mathsf{SNR}_{\mathsf{ideal}}(f)$ is defined in (29).

Proposed upper bound (Shannon and Bode/Fano): This upper bound is obtained as a solution to problem (31) which maximizes the achievable rate over all physically realizable matching networks at transmitter.

Conjugate matching at center frequency: The main objective of the conjugate matching scheme is to ensure optimal power transfer at the center frequency, i.e., $\mathcal{T}(f_{\mathsf{c}}) = 1$. The matching network is designed using the L matching scheme from [5, Section 6.5] such that the load impedance and source impedance are complex conjugates at the center frequency. At center frequency, the impedance of the equivalent load can be modeled as a capacitor C_{center} in series with a resistor R_{center}. As $R_{\mathsf{center}} < R$, the quality factor value is set as $Q = \sqrt{\frac{R}{R_{\mathsf{center}}} - 1}$. By fixing this quality factor and using an LC ladder matching topology as shown in Fig. 3 with just one LC block, we obtain

$$L_1 = \frac{QR_{\mathsf{center}}}{2\pi f_{\mathsf{c}}} + \frac{1}{4\pi^2 f_{\mathsf{c}}^2 C_{\mathsf{center}}}, \tag{43a}$$

$$C_1 = \frac{Q}{2\pi f_{\mathsf{c}} R}. \tag{43b}$$

The transmission coefficient for conjugate matching circuit equals 1 at the center frequency as shown in Fig. 4 and Fig. 5.

Proposed optimal transmission (circuit in ADS): This case corresponds to the optimized matching network design obtained through the three step procedure in Section IV-A. The third step in this procedure is sub-optimal because it is based on an iterative numerical solver from the ADS optimization toolbox.

Benchmark of frequency-flat transmission coefficient: This case corresponds to the frequency-flat transmission coefficient

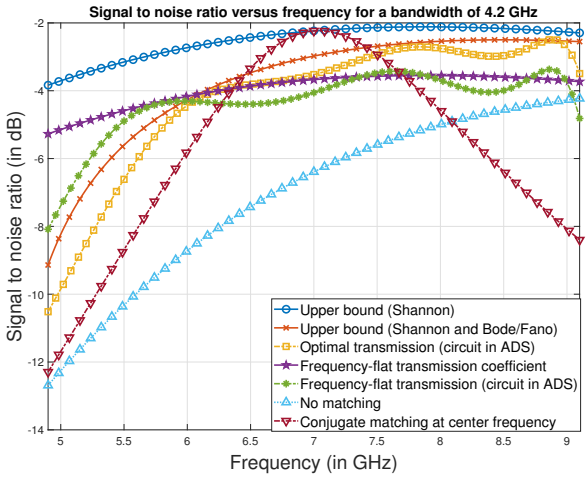

(a) Bandwidth of 4.2 GHz.

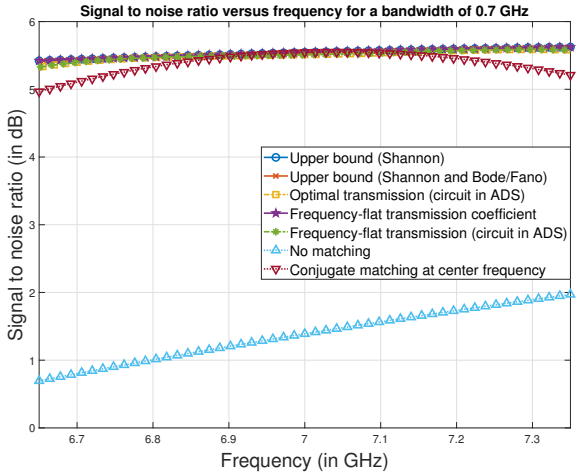

(b) Bandwidth of 0.7 GHz.

Fig. 6: For a single Chu's antenna: In (a), the SNR curve for the optimal transmission ADS circuit is higher than the frequency-flat transmission curve for frequencies above 6.1 GHz. In (b), the SNR curves for the optimal and frequency-flat transmission coincide.

$\mathcal{T}_{\text{ff}}$ derived using (42) (also known as box-car matching approach in [15]).

Benchmark of frequency-flat transmission (circuit in ADS): The matching network is designed to approximate the frequency-flat coefficient $\mathcal{T}_{\text{ff}}$ satisfying Bode-Fano constraints.

Benchmark of no matching: Finally, we also compare with the case when matching network is absent, i.e., the source is directly connected to the antenna array. The resulting SNR is defined as

$$\text{SNR}_{\text{No-match}}(f) = \frac{|\mathbf{s}_{\text{RT}}^{T}(f)(\mathbf{I} - \mathbf{S}_{\text{F},22}(f)\mathbf{S}_{\text{T}}(f))^{-1}\mathbf{s}_{\text{F},21}(f)|^2 \text{E}_{\text{s}}}{\text{N}_0}. \tag{44}$$

A. Simulation results for a single Chu's antenna

In Fig. 6(a), we use the parameter setup and the transmission coefficient based on circuit design in Section IV-B for computing the SNR versus frequency for the seven cases. We observe that the SNR solely based on Shannon's upper bound is higher than that of the bound which incorporates Bode-Fano wideband matching theory. The Shannon upper bound technique overestimates the SNR. This upper bound cannot be attained by any practical matching network. The bound proposed by combining Shannon's theory and Bode-Fano theory is more realistic as it incorporates the gain-bandwidth tradeoff in matching networks. We show that this bound can be approximated using a practical matching network topology optimized using ADS as discussed in Section IV-B. For a

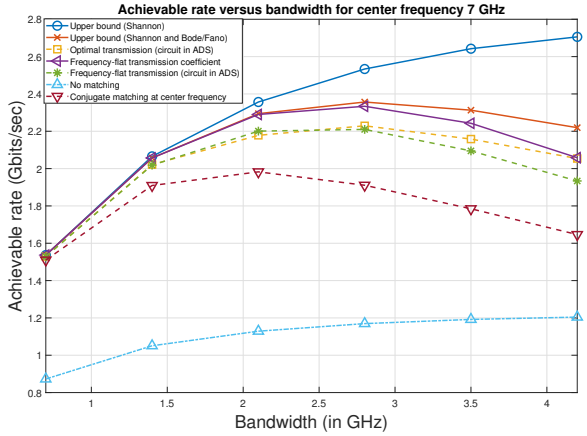

Fig. 7: Achievable rate versus bandwidth for a single Chu's antenna with center frequency 7 GHz. The circuit based on optimal transmission significantly outperforms the frequency-flat transmission circuit for larger bandwidths. Also, the optimal bandwidth for getting the highest achievable rate is 2.8 GHz beyond which rate decreases.

major portion of the 4.2 GHz bandwidth, the SNR for the ADS circuit corresponding to the optimal transmission is greater than that of the frequency-flat transmission circuit. This leads to a higher achievable rate as well for the optimal transmission based circuit. The SNR corresponding to the conjugate matching network is higher than the optimal transmission for frequencies 6.5 GHz to 7.4 GHz but drastically decreases outside this range. As rate depends on the SNR for the whole band from 4.9 GHz to 9.1 GHz, the achievable rate for conjugate matching is less than the rate for optimal transmission and frequency-flat transmission. Even for a bandwidth of 0.7 GHz as shown in Fig. 6(b), conjugate matching is still worse compared to the proposed approach because the optimal transmission solution in (34a) depends on bandwidth unlike conjugate matching as shown in Fig. 4.

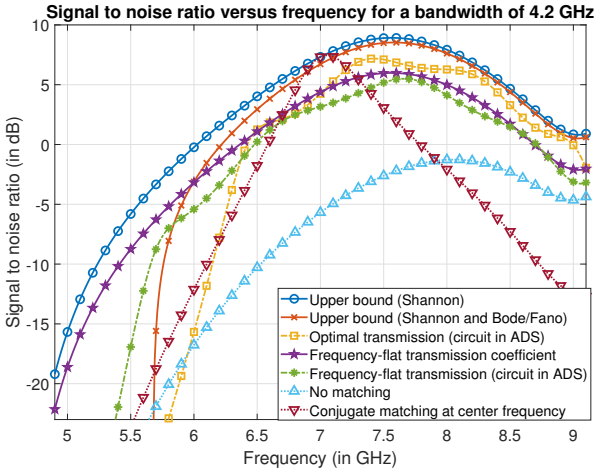

(a) Beamforming off-broadside at $\theta = \frac{\pi}{4}$

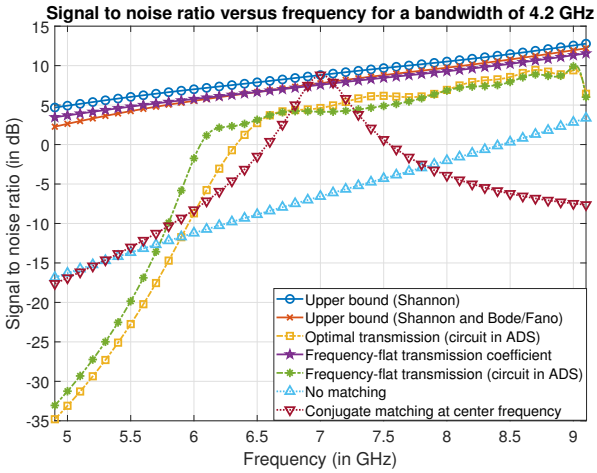

(b) Beamforming at broadside, i.e., $\theta = 0$

Fig. 8: For an array with $N = 8$ dipole antennas with frequency-flat analog beamforming. SNR degradation for $\theta = \frac{\pi}{4}$ compared to $\theta = 0$ because of beam squint effect.

In Fig. 7, we plot the achievable rate as a function of bandwidth. The achievable rate plot based on the Shannon upper bound continuously increases with the bandwidth. A realistic trend is observed for the upper bound obtained after incorporating Bode-Fano theory, i.e., we observe that the rate decreases beyond a certain bandwidth. The results highlight how the matching network limits the bandwidth and achievable rate of the system. We show the existence of an optimal bandwidth which gives the highest possible achievable rate because of the gain-bandwidth tradeoff of matching networks. From the proposed upper bound plot and the corresponding ADS circuit simulation, the optimal bandwidth for highest achievable rate is 2.8 GHz. For conjugate matching, this optimal bandwidth is 2.1 GHz. It is lower than the optimal bandwidth of the

proposed ADS circuit because conjugate matching response is invariant of the bandwidth. The proposed matching approach accounts for the bandwidth dependence and enables use of higher bandwidth for maximizing rate. Comparing with the frequency-flat transmission coefficient approach from [15], we see that the proposed optimal transmission approach performs better beyond 2.8 GHz. At higher bandwidths, more power is transferred through the matching network for frequencies with higher $\mathsf{SNR}_{\text{ideal}}(f)$. Below 2.8 GHz bandwidth, the rate performance of the optimal transmission is nearly same as frequency-flat transmission.

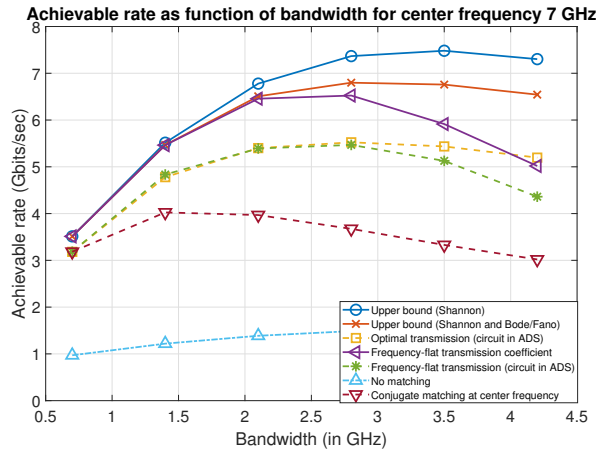

(a) Beamforming off-broadside at $\theta = \frac{\pi}{4}$

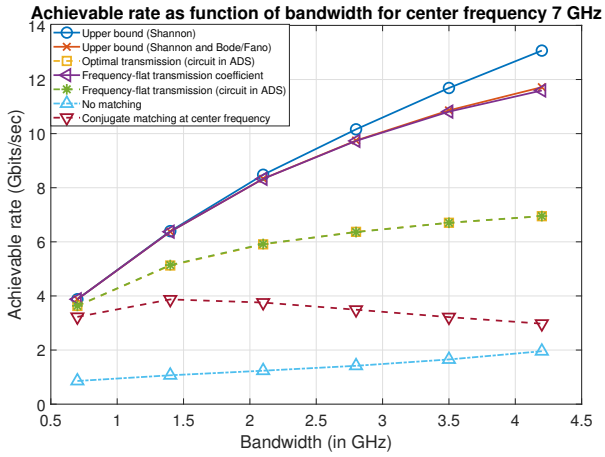

(b) Beamforming at broadside, i.e., $\theta = 0$

Fig. 9: Achievable rate versus bandwidth for an array with $N = 8$ dipole antennas with broadside and off-broadside analog beamforming. At larger bandwidths, achievable rates of beamforming off-broadside are lower than broadside beamforming because of beam squint.

B. Simulation results for an array of dipole antennas

In Fig. 8, we use the parameter setup and the transmission coefficient based on circuit design in Section IV-C for computing the SNR versus frequency for the seven cases. Most of the SNR comparison and trends are similar to that discussed in Section V-A. At broadside incidence, i.e., $\theta = 0$, there is no relative phase difference between two antennas. Hence, frequency-flat beamforming works well. For off-broadside incidence, i.e., $\theta = \frac{\pi}{4}$, the phase-difference between two antennas varies as a function of frequency as shown in (41). Using a frequency-flat beamforming for off-broadside at higher bandwidths results in a phase mismatch and subsequent SNR reduction. This effect is commonly known as beam squint. So, we observe SNR degradation for off-broadside compared to broadside in Fig. 8.

In Fig. 9, for $\theta = \frac{\pi}{4}$, we observe that the achievable rate corresponding to the frequency-flat transmission decreases beyond 2.8 GHz whereas the proposed optimal transmission bound as well as circuit performs better. For $\theta = 0$, the achievable rate increases faster with bandwidth compared to $\theta = \frac{\pi}{4}$ because there is no phase mismatch. Frequency-selective true time delay (TTD) beamforming can be used to mitigate the beam squint effect. The achievable rate variation with bandwidth for TTD systems is a future direction.

From the achievable rate results in Fig. 7 and Fig. 9, we see that the rate corresponding to the proposed optimal transmission coefficient is higher than the baseline frequency-flat transmission coefficient from [15] especially for larger bandwidths because $\mathcal{T}^{\star}(f)$ is higher for frequencies with better $\mathsf{SNR}_{\text{ideal}}(f)$ unlike $\mathcal{T}_{\text{ff}}$ which is frequency-flat and does not depend on $\mathsf{SNR}_{\text{ideal}}(f)$. Both optimal and frequency-flat transmission coefficient provide higher rate than the conjugate matching scheme for all bandwidths because conjugate matching solution is based on providing optimal power transfer only at the center frequency, i.e., $\mathcal{T}(f_{\text{c}}) = 1$. Moreover, the conjugate matching solution is independent of the bandwidth unlike $\mathcal{T}^{\star}(f)$ and $\mathcal{T}_{\text{ff}}$ which depend on the bandwidth. As a result, conjugate matching is increasingly inefficient as bandwidth grows wider.

C. Comparison of equal power allocation and water-filling over frequency for $\mathsf{E_s}(f)$

In the previous simulations, we used an equal power allocation scheme, i.e., $\mathsf{E_s}(f)$ was frequency flat and set to $\mathsf{E_s}(f) \equiv \mathsf{E_s} = \frac{0.25}{B}\left[\frac{\text{W}}{\text{Hz}}\right]$. These plots from Fig. 9a are labeled as 'EPA' (Equal power allocation) in Fig. 10. We now analyze the case where $\mathsf{E_s}(f)$ is frequency-selective and optimally designed using the water-filling (WF) algorithm [7]. We optimize $\mathsf{E_s}(f)$ based on the following problem.

$$\mathsf{E_s}^{\star}(f) = \underset{\mathsf{E_s}(f)}{\text{argmax}} \int_{f_{\text{min}}}^{f_{\text{max}}} \log_2\left(1 + \frac{\mathsf{SNR}_{\text{ideal}}(f)}{\mathsf{E_s}}\mathsf{E_s}(f)\right) \mathrm{d}f, \tag{45a}$$

$$\text{s.t.} \int_{f_{\text{min}}}^{f_{\text{max}}} \mathsf{E_s}(f)\mathrm{d}f \leq 0.25, \tag{45b}$$

$$\mathsf{E_s}(f) \geq 0. \tag{45c}$$

The optimal solution for this problem is defined in terms of the Lagrangian parameter η as

$$\mathsf{E_s}^{\star}(f) = \left(\frac{1}{\eta} - \frac{\mathsf{E_s}}{\mathsf{SNR}_{\text{ideal}}(f)}\right)^{+}, \tag{46}$$

where η is found numerically using bisection search to satisfy $\int_{f_{\text{min}}}^{f_{\text{max}}} \mathsf{E_s}^{\star}(f)\mathrm{d}f = 0.25$ within a threshold.

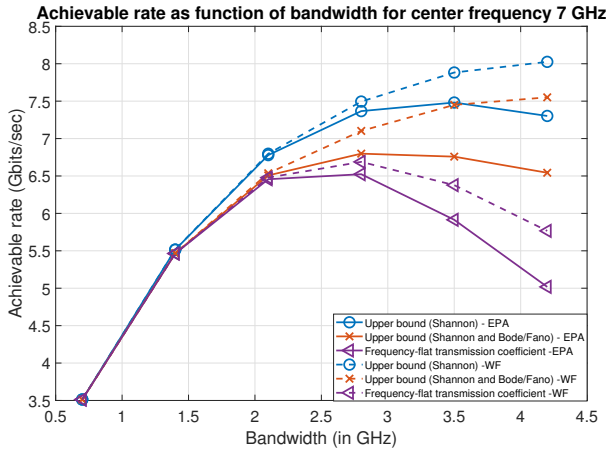

Fig. 10: Achievable rate versus bandwidth for a dipole array with center frequency 7 GHz. Water-filling approach outperforms equal power allocation approach especially at larger bandwidths because more power is allocated to frequencies with higher $\mathsf{SNR}_{\text{ideal}}(f)$.

We now compute $\mathsf{R}_{\max}$ using $\mathsf{E}_{\mathsf{s}}^{\star}(f)$ from (46) instead of frequency-flat E_{s}. The plots corresponding to $\mathsf{E}_{\mathsf{s}}^{\star}(f)$ are labeled as 'WF' in Fig. 10. We observe that the achievable rate for 'EPA' and 'WF' are similar upto 2.1 GHz bandwidth. Beyond 2.1 GHz bandwidth, we see that the 'WF' approach performs better than 'EPA' for all three cases. The achievable rate performance is improved because 'WF' approach allocates more power to frequencies with higher values of $\mathsf{SNR}_{\text{ideal}}(f)$.

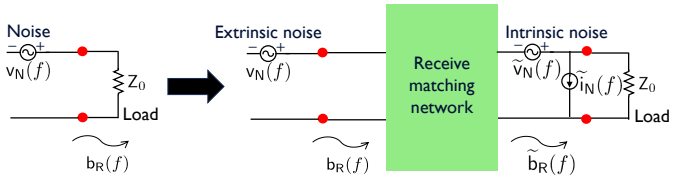

Fig. 11: Extrinsic noise and signal component in $\mathsf{b}_{\mathsf{R}}(f)$ are equally impacted by the receive matching network whereas intrinsic noise component is not impacted by receive matching.

D. Impact of receiver matching network and intrinsic noise

To study the impact of receiver matching network and intrinsic noise, let us assume a system model shown in Fig. 11, where the modified receiver model includes a receive matching network block and intrinsic noise sources $\widetilde{\mathsf{v}}_{\mathsf{N}}(f)$ and $\widetilde{\mathsf{i}}_{\mathsf{N}}(f)$ [17]. The resulting root power wave incident on the load after passing through the receive matching network is $\widetilde{\mathsf{b}}_{\mathsf{R}}(f)$. Let the transmission coefficient at the receiver be defined as

$$\mathcal{T}_{\mathsf{rx}}(f) = \frac{\mathbb{E}[|\widetilde{\mathsf{b}}_{\mathsf{R}}(f)|^2]}{\mathbb{E}[|\mathsf{b}_{\mathsf{R}}(f)|^2]}. \tag{47}$$

For the sake of simplicity in simulations, we assume that $\mathcal{T}_{\mathsf{rx}}(f)$ is frequency-flat and set to $\mathcal{T}_{\mathsf{rx}}(f) \equiv \mathcal{T}_{\mathsf{rx}}$.

For the LNA, let the noise factor $\mathsf{NF} = 2$ as in [22]. As intrinsic noise is added after the receiver matching block, it is not impacted by $\mathcal{T}_{\mathsf{rx}}$. The intrinsic noise contribution is $\mathsf{N}_{\mathsf{LNA}} = \mathsf{N}_0(\mathsf{NF}-1)$ [22]. Both signal and extrinsic noise components in $\mathsf{b}_{\mathsf{R}}(f)$ are equally impacted by the receiver matching block. The total noise is $\mathcal{T}_{\mathsf{rx}}\mathsf{N}_0 + \mathsf{N}_{\mathsf{LNA}} = \mathsf{N}_0(\mathcal{T}_{\mathsf{rx}} + \mathsf{NF} - 1)$. Hence, the resulting receive SNR incorporating receiver matching network and intrinsic noise is defined as

$$\widetilde{\mathsf{SNR}}(f) = \mathsf{SNR}_{\text{ideal}}(f)\mathcal{T}(f)\frac{\mathcal{T}_{\mathsf{rx}}}{\mathcal{T}_{\mathsf{rx}} + \mathsf{NF} - 1}. \tag{48}$$

From (48), we see that the resulting SNR is scaled by the factor $\frac{\mathcal{T}_{\mathsf{rx}}}{\mathcal{T}_{\mathsf{rx}}+\mathsf{NF}-1} < 1$. Hence, the SNR and the achievable rate obtained after incorporating transmit matching, receiver matching, and intrinsic noise is lowered compared to the case when only transmit matching network is included. We verify this in Fig. 12 where the achievable rate for $\mathcal{T}_{\mathsf{rx}} = 0.7$ is lower than the case of the ideal receiver. We also observe that the inclusion of receive matching network and intrinsic noise only lowers the achievable rate but does not change the achievable rate trend with bandwidth. Hence, the insights and comparison trends from previous simulations are also valid for a practical receiver.

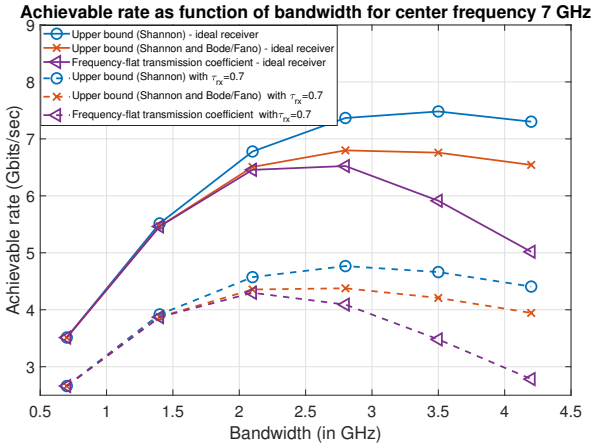

Fig. 12: Achievable rate versus bandwidth for a dipole array with center frequency 7 GHz. Modeling transmission coefficient $\mathcal{T}_{\mathsf{rx}}$ for receive matching network lowers the achievable rate but does not change the bandwidth trend. This ensures generalization of the insights from previous simulations to a practical receiver.

VI. Conclusion

In this paper, we generalized the achievable rate analysis for a MISO system by incorporating constraints from Bode-Fano wideband matching theory. We proposed a general optimization framework which maximizes the achievable rate over all physically realizable linear and passive matching networks. The proposed upper bound based on the combination of Shannon's theory and Bode-Fano theory is more realistic because it captures the gain-bandwidth tradeoff of matching networks. We also proposed a simple three step procedure to design matching networks that approximate this bound. We demonstrated this procedure for a single Chu's antenna and an array with dipole antennas. From the derived theoretical bound and the ADS circuit simulations, an optimal bandwidth behavior is observed in the achievable rate analysis as function of the bandwidth.

TABLE I: Evaluation of $\xi_{\mathsf{BF},i}(f)$ and $B_{\mathsf{BF},i}$ (Based on [2, Table 1])

Location in WCP	$\xi_{\mathsf{BF},i}(f)$	$B_{\mathsf{BF},i}$
$s_i = \mathrm{j}2\pi f_i$	$\frac{1}{4\pi^2}\left[\frac{1}{(f_i-f)^2}+\frac{1}{(f_i+f)^2}\right]$	$-\left[\sum_{\ell=1}^{N_\mathsf{p}}(p_{\mathsf{eq},\ell}-\mathrm{j}2\pi f_i)^{-1}+\sum_{m=1}^{N_\mathsf{z}}(z_{\mathsf{eq},m}+\mathrm{j}2\pi f_i)^{-1}\right]$
$\mathcal{R}\{s_i\} > 0$	$\mathcal{R}\{(s_i-\mathrm{j}2\pi f_i)^{-1}+(s_i+\mathrm{j}2\pi f_i)^{-1}\}$	$-\log\left(\left\lvert\hat{\mathsf{S}}_{\mathsf{eq}}(s_i)\frac{\prod_{m=1}^{N_\mathsf{z}}(s_i+z_{\mathsf{eq},m})}{\prod_{m=1}^{N_\mathsf{z}}(s_i-z_{\mathsf{eq},m})}\right\rvert\right)$
$s_i = \infty$	1	$\frac{-1}{2}\left[\sum_{\ell=1}^{N_\mathsf{p}}p_{\mathsf{eq},\ell}+\sum_{m=1}^{N_\mathsf{z}}z_{\mathsf{eq},m}\right]$

In future work, we propose the application of this methodology to other antenna types like patch antenna. The main challenge is to numerically compute the upper bound because the number of Bode-Fano constraints increases for complicated antenna geometries. In future work, we plan to extend this work to MIMO systems with multiple RF chains and study the bandwidth-multiplexing tradeoff [31]. For $\mathsf{N_{RF}}$ number of RF chains, the two-port matching network will expand to $2\mathsf{N_{RF}} \times 2\mathsf{N_{RF}}$ matrix. This will lead to a transmission coefficient matrix instead of a scalar transmission coefficient. The formulation and optimization for the $\mathsf{N_{RF}}$ RF chain system is a direction for future work. Another open challenge in extension to MIMO is the joint optimization of multiport transmit and receive impedance-matching networks.

Appendix A
Computing the scattering parameter $\hat{\mathsf{S}}_{\mathsf{eq}}(s)$ in rational form [31]

Case 1: The impedance parameter of the load is analytically known in the rational form in the whole complex plane and denoted as $\hat{\mathsf{Z}}_{\mathsf{eq}}(s)$. The corresponding scattering parameter of the load in the rational form is

$$\hat{\mathsf{S}}_{\mathsf{eq}}(s) = \frac{\hat{\mathsf{Z}}_{\mathsf{eq}}(s) - \mathsf{Z}_0}{\hat{\mathsf{Z}}_{\mathsf{eq}}(s) + \mathsf{Z}_0}. \tag{49}$$

Case 2: The measured value of the scattering parameter of the load $\mathsf{S}_{\mathsf{eq}}(f)$ is available for the frequency f in the range of interest $[f_1, f_2]$. A passive and rational approximation $\hat{\mathsf{S}}_{\mathsf{eq}}(s)$ is obtained such that $\hat{\mathsf{S}}_{\mathsf{eq}}(\mathrm{j}2\pi f)$ is close to $\mathsf{S}_{\mathsf{eq}}(f)$ for $f \in [f_1, f_2]$ within a specified error tolerance. This can be done numerically using the *rationalfit* function in MATLAB [45].

Appendix B
Computing $\xi_{\mathsf{BF},i}(f)$ and $B_{\mathsf{BF},i}$ for $\{i\}_1^{N_{\mathsf{BF}}}$ from $\hat{\mathsf{S}}_{\mathsf{eq}}(s)$

Using closed-form expression of $\hat{\mathsf{S}}_{\mathsf{eq}}(s)$, we first solve the following for s [2].

$$\hat{\mathsf{S}}_{\mathsf{eq}}(-s)\hat{\mathsf{S}}_{\mathsf{eq}}(s) - 1 = 0. \tag{50}$$

Let s_i be a distinct root of (50). The value of s_i in (50) can be obtained analytically or numerically by using *vpasolve* function in MATLAB. Let $\{z_{\mathsf{eq},1}, \ldots, z_{\mathsf{eq},m}, \ldots, z_{\mathsf{eq},N_\mathsf{z}}\}$ be the zeros and $\{p_{\mathsf{eq},1}, \ldots, p_{\mathsf{eq},\ell}, \ldots, p_{\mathsf{eq},N_\mathsf{p}}\}$ be the poles of the rational equivalent load $\hat{\mathsf{S}}_{\mathsf{eq}}(s)$. For each s_i, there is a corresponding $\xi_{\mathsf{BF},i}(f)$ and $B_{\mathsf{BF},i}$ depending on the location of s_i in the whole complex plane (WCP) categorized in Table I. For the case of multiplicity of s_i more than one, i.e. there are repeated roots, $\xi_{\mathsf{BF},i}(f)$ and $B_{\mathsf{BF},i}$ can be computed using [31, Eq 21- Eq 23] for each repeated root.

Appendix C
Proof of Theorem 2

The variables $\mathcal{T}^\star(f)$ and $\mu_i^\star|_{i=1}^{N_{\mathsf{BF}}+2}$ satisfy the KKT conditions [22], [41] applied to (31).

Primal feasibility:

$$\int_0^\infty \xi_{\mathsf{BF},i}(f)\log\left(\frac{1}{1-\mathcal{T}^\star(f)}\right)\mathrm{d}f - B_{\mathsf{BF},i} \le 0, \{i\}_1^{N_{\mathsf{BF}}}, \tag{51a}$$

$$\mathcal{T}^\star(f) - 1 \le 0, \tag{51b}$$

$$-\mathcal{T}^\star(f) \le 0. \tag{51c}$$

Dual feasibility: $\mu_i^\star \ge 0$.

Complementary slackness:

$$\mu_i^\star\left(\int_0^\infty \xi_{\mathsf{BF},i}(f)\log\left(\frac{1}{1-\mathcal{T}^\star(f)}\right)\mathrm{d}f - B_{\mathsf{BF},i}\right) = 0, \{i\}_1^{N_{\mathsf{BF}}} \tag{52a}$$

$$\mu_{N_{\mathsf{BF}}+1}^\star \mathcal{T}^\star(f) = 0, \tag{52b}$$

$$\mu_{N_{\mathsf{BF}}+2}^\star(\mathcal{T}^\star(f) - 1) = 0. \tag{52c}$$

Stationarity: Let $\chi(f)$ be an arbitrary shaped function and ϵ represents the magnitude of variation [22]. Using variational calculus and the stationarity condition, we set $\frac{\mathrm{d}}{\mathrm{d}\epsilon}\left[\mathcal{L}\left(\mathcal{T}^\star(f)+\epsilon\chi(f)\right)\right]\Big|_{\epsilon=0} = 0$, simplified using chain rule as

$$\begin{aligned}
&= \frac{\mathrm{d}\left(\mathcal{T}^\star(f)+\epsilon\chi(f)\right)}{\mathrm{d}\epsilon}\frac{\mathrm{d}\left[\mathcal{L}\left(\mathcal{T}^\star(f)+\epsilon\chi(f)\right)\right]\Big|_{\epsilon=0}}{\mathrm{d}\left(\mathcal{T}^\star(f)+\epsilon\chi(f)\right)} \\
&= \frac{\mathrm{d}\left[\mathcal{L}\left(\mathcal{T}^\star(f)+\epsilon\chi(f)\right)\right]}{\mathrm{d}\left(\mathcal{T}^\star(f)+\epsilon\chi(f)\right)}\chi(f)\Big|_{\epsilon=0} \\
&\overset{(a)}{=} \int_0^\infty \frac{\chi(f)}{\ln 2}\left[\left(\frac{-\mathsf{SNR}_{\mathsf{ideal}}(f)}{1+\mathsf{SNR}_{\mathsf{ideal}}(f)\mathcal{T}^\star(f)}\right)+\right. \\
&\left.\sum_{i=1}^{N_{\mathsf{BF}}}\mu_i^\star\frac{\ln 2\xi_{\mathsf{BF},i}(f)}{(1-\mathcal{T}^\star(f))}\right]\mathrm{d}f - \mu_{N_{\mathsf{BF}}+1}^\star\chi(f) + \mu_{N_{\mathsf{BF}}+2}^\star\chi(f),
\end{aligned} \tag{53}$$

where (a) follows from (32). Let $\mu_{N_{\mathsf{BF}}+1}^\star = 0$ and $\mu_{N_{\mathsf{BF}}+2}^\star = 0$ to satisfy (52b) and (52c) respectively. Setting $\mu_{N_{\mathsf{BF}}+2}^\star = 0$ allows $\mathcal{T}(f) < 1$ for any finite frequency range which is required for the Bode-Fano integral in (51a) to be bounded. Note that $\mathcal{T}(f) = 1$ is possible only at a discrete point. For example, in the case of conjugate matching at center frequency, $\mathcal{T}(f_\mathsf{c}) = 1$. Equating (53) to 0 is equivalent to setting the integrand inside the integral to 0. As $\chi(f)$ is an arbitrary function, the non-trivial condition is

$$\left[\left(\frac{-\mathsf{SNR}_{\mathsf{ideal}}(f)}{1+\mathsf{SNR}_{\mathsf{ideal}}(f)\mathcal{T}^\star(f)}\right)+\sum_{i=1}^{N_{\mathsf{BF}}}\mu_i^\star\frac{\ln 2\xi_{\mathsf{BF},i}(f)}{(1-\mathcal{T}^\star(f))}\right] = 0. \tag{54}$$

Simplifying (54), we obtain

$$\mathcal{T}^{\star}(f)\left(1+\ln 2\sum_{i=1}^{N_{\mathsf{BF}}}\mu_i^{\star}\xi_{\mathsf{BF},i}(f)\right)=1-\frac{\ln 2\sum_{i=1}^{N_{\mathsf{BF}}}\mu_i^{\star}\xi_{\mathsf{BF},i}(f)}{\mathsf{SNR}_{\mathsf{ideal}}(f)}. \tag{55}$$

For (51a) to be satisfied, $\mathcal{T}^{\star}(f)-1\leq 0$ which requires atleast one $\mu_i^{\star}$ to be strictly positive based on the expression of $\mathcal{T}^{\star}(f)$ from (55). Combining (51c) and (55), we get (34a).

REFERENCES

[1] B. K. Lau, J. Andersen, G. Kristensson, and A. Molisch, "Impact of matching network on bandwidth of compact antenna arrays," *IEEE Trans. Antennas Propag.*, vol. 54, no. 11, pp. 3225–3238, Nov. 2006.

[2] D. Nie and B. M. Hochwald, "Bandwidth analysis of multiport radio frequency systems—part I," *IEEE Trans. Antennas Propag.*, vol. 65, no. 3, pp. 1081–1092, Mar. 2017.

[3] P. S. Taluja and B. L. Hughes, "Bandwidth limitations and broadband matching for coupled multi-antenna systems," in *Proc. IEEE Globecom*. Houston, TX, USA: IEEE, Dec. 2011, pp. 1–6.

[4] S. Saab, A. Mezghani, and R. W. Heath, "Optimizing the mutual information of frequency-selective multi-port antenna arrays in the presence of mutual coupling," *IEEE Trans. Commun.*, vol. 70, no. 3, pp. 2072–2084, Mar. 2022.

[5] M. Steer, *Microwave and RF design (Third Edition, 2019)*. NC State University, 2019.

[6] S. Park, A. Alkhateeb, and R. W. Heath, "Dynamic subarrays for hybrid precoding in wideband mmWave MIMO systems," *IEEE Trans. Wirel. Commun.*, vol. 16, no. 5, pp. 2907–2920, May 2017.

[7] R. W. Heath Jr and A. Lozano, *Foundations of MIMO Communication*, 1st ed. Cambridge University Press, Dec. 2018.

[8] H. W. Bode *et al.*, "Network analysis and feedback amplifier design," 1945.

[9] R. M. Fano, "Theoretical limitations on the broadband matching of arbitrary impedances," *Journal of the Franklin Institute*, vol. 249, no. 1, pp. 57–83, 1950.

[10] C. R. Chappidi and K. Sengupta, "Globally optimal matching networks with lossy passives and efficiency bounds," *IEEE Trans. Circuits Syst. I: Regul. Pap.*, vol. 65, no. 1, pp. 257–269, 2018.

[11] D. Nie, B. M. Hochwald, and E. Stauffer, "Systematic design of large-scale multiport decoupling networks," *IEEE Trans. Circuits Syst. I: Regul. Pap.*, vol. 61, no. 7, pp. 2172–2181, Jul. 2014.

[12] N. Deshpande, M. R. Castellanos, S. R. Khosravirad, J. Du, H. Viswanathan, and R. W. Heath, "A wideband generalization of the near-field region for extremely large phased-arrays," *IEEE Wireless Commun. Lett.*, vol. 12, no. 3, pp. 515–519, 2023.

[13] M. Cai, K. Gao, D. Nie, B. Hochwald, J. N. Laneman, H. Huang, and K. Liu, "Effect of wideband beam squint on codebook design in phased-array wireless systems," in *Proc. IEEE Globecom*, 2016, pp. 1–6.

[14] N. V. Deshpande, S. R. Khosravirad, J. Du, H. Viswanathan, M. R. Castellanos, and R. W. Heath, "Analysis of dense array massive MIMO with practical constraints," in *Proc. 26th Int. ITG Workshop Smart Antennas and 13th Conference on Systems, Communications, and Coding*. VDE, 2023, pp. 1–6.

[15] P. S. Taluja and B. L. Hughes, "Diversity limits of compact broadband multi-antenna systems," *IEEE J. Sel. Areas Commun.*, vol. 31, no. 2, p. 12, 2013.

[16] B. Wang, F. Gao, S. Jin, H. Lin, and G. Y. Li, "Spatial- and frequency-wideband effects in millimeter-wave massive MIMO systems," *IEEE Trans. Signal Process.*, vol. 66, no. 13, pp. 3393–3406, 2018.

[17] M. T. Ivrlac and J. A. Nossek, "Toward a circuit theory of communication," *IEEE Trans. Circuits Syst. I: Regul. Pap.*, vol. 57, no. 7, pp. 1663–1683, Jul. 2010.

[18] T. A. de Vasconcelos, A. L. F. de Almeida, and J. A. Nossek, "Matching strategies for multiantenna arrays," in *Proc. 24th Int. ITG Workshop Smart Antennas (WSA)*, 2020, pp. 1–6.

[19] T. L. Marzetta, "Super-directive antenna arrays: Fundamentals and new perspectives," in *Proc. 53rd Asilomar Conf. Signals, Syst., Comput.*, 2019, pp. 1–4.

[20] J. Wallace and M. Jensen, "Mutual coupling in MIMO wireless systems: A rigorous network theory analysis," *IEEE Trans. Wirel. Commun.*, vol. 3, no. 4, pp. 1317–1325, Jul. 2004.

[21] L. Kundu and B. L. Hughes, "Enhancing capacity in compact MIMO-OFDM systems with frequency-selective matching," *IEEE Trans. Commun.*, vol. 65, no. 11, pp. 4694–4703, Nov. 2017.

[22] V. Shyianov, M. Akrout, F. Bellili, A. Mezghani, and R. W. Heath, "Achievable rate with antenna size constraint: Shannon meets Chu and Bode," *IEEE Trans. Commun.*, vol. 70, no. 3, pp. 2010–2024, Mar. 2022.

[23] M. Akrout, V. Shyianov, F. Bellili, A. Mezghani, and R. W. Heath, "Super-wideband massive mimo," *arXiv preprint arXiv:2208.01556*, 2022.

[24] M. Akrout, F. Bellili, A. Mezghani, and J. A. Nossek, "Physically consistent models for intelligent reflective surface-assisted communications under mutual coupling and element size constraint," *arXiv preprint arXiv:2302.11130*, 2023.

[25] L. J. Chu, "Physical limitations of omni-directional antennas," *Journal of applied physics*, vol. 19, no. 12, pp. 1163–1175, 1948.

[26] C. A. Balanis, *Antenna theory: analysis and design*. John wiley & sons, 2015.

[27] P. R. Gray, P. J. Hurst, S. H. Lewis, and R. G. Meyer, *Analysis and design of analog integrated circuits*. John Wiley & Sons, 2009.

[28] S. Saab, A. Mezghani, and R. W. Heath, "Capacity based optimization of compact wideband antennas," in *Proc. IEEE-APS Topical Conf. Antennas Propag. Wireless Commun. (APWC)*. Granada, Spain: IEEE, Sep. 2019, pp. 322–325.

[29] ——, "Capacity based analysis of a wideband SIMO system in the presence of mutual coupling," in *Proc. IEEE Globecom*. Waikoloa, HI, USA: IEEE, Dec. 2019, pp. 1–6.

[30] N. Deshpande, M. R. Castellanos, S. R. Khosravirad, J. Du, H. Viswanathan, and R. W. Heath, "Achievable rate of a SISO system under wideband matching network constraints," in *Proc. IEEE Globecom*. Kuala Lumpur, Malaysia: IEEE, Dec. 2023, pp. 7514–7519.

[31] D. Nie and B. M. Hochwald, "Bandwidth analysis of multiport radio-frequency systems—part II," *IEEE Trans. Antennas Propag.*, vol. 65, no. 3, pp. 1093–1107, Mar. 2017.

[32] N. Decarli, "On phase-based localization with narrowband backscatter signals," *EURASIP J. Adv. Signal Process*, vol. 2018, no. 1, pp. 1–12, 2018.

[33] K. Kousias, G. Caso, O. Alay, A. Brunstrom, L. D. Nardis, M.-G. D. Benedetto, and M. Neri, "Coverage and deployment analysis of narrowband internet of things in the wild," *IEEE Commun. Mag.*, vol. 58, no. 9, pp. 39–45, 2020.

[34] C. Han, A. O. Bicen, and I. F. Akyildiz, "Multi-ray channel modeling and wideband characterization for wireless communications in the Terahertz band," *IEEE Trans. Wirel. Commun.*, vol. 14, no. 5, pp. 2402–2412, 2015.

[35] R. J. Williams, P. Ramírez-Espinosa, J. Yuan, and E. de Carvalho, "Electromagnetic based communication model for dynamic metasurface antennas," *IEEE Trans. Wirel. Commun.*, vol. 21, no. 10, pp. 8616–8630, 2022.

[36] M. R. Castellanos and R. W. Heath, "MIMO communication with polarization reconfigurable antennas," in *Proc. 55th Asilomar Conf. Signals, Syst., Comput.*, 2021, pp. 427–431.

[37] W. B. Davenport, W. L. Root *et al.*, *An introduction to the theory of random signals and noise*. McGraw-Hill New York, 1958, vol. 159.

[38] J. A. Russer and P. Russer, "Modeling of noisy EM field propagation using correlation information," *IEEE Trans. Microw. Theory Tech.*, vol. 63, no. 1, pp. 76–89, 2014.

[39] D. Williams, "Traveling waves and power waves: Building a solid foundation for microwave circuit theory," *IEEE Microw. Mag.*, vol. 14, no. 7, pp. 38–45, 2013.

[40] S. Darlington, "Synthesis of reactance 4-poles which produce prescribed insertion loss characteristics: including special applications to filter design," *Journal of Mathematics and Physics*, vol. 18, no. 1-4, pp. 257–353, 1939.

[41] S. Boyd, S. P. Boyd, and L. Vandenberghe, *Convex optimization*. Cambridge university press, 2004.

[42] C. Shannon, "Communication in the presence of noise," *Proceedings of the IRE*, vol. 37, no. 1, pp. 10–21, 1949.

[43] P. He and L. Zhao, "Generalized water-filling for sum power minimization with peak power constraints," in *2015 International Conference on Wireless Communications & Signal Processing (WCSP)*. IEEE, 2015.

[44] Agilent Technologies. (2011) Advanced Design System 2011.01 - Tuning, Optimization, and Statistical Design. [Online]. Available: https://edadownload.software.keysight.com/eedl/ads/2011_01/pdf/optstat.pdf

[45] B. Gustavsen and A. Semlyen, "Rational approximation of frequency domain responses by vector fitting," *IEEE Trans. Power Deliv.*, vol. 14, no. 3, pp. 1052–1061, 1999.